SIMPLE CHEMICAL ROUTES FOR CHANGING COMPOSITION OR MORPHOLOGY IN METAL CHALCOGENIDE NANOMATERIALS

A Dissertation

by

STACEY ELAINE WARK

Submitted to the Office of Graduate Studies of
Texas A&M University
in partial fulfillment of the requirements for the degree of

DOCTOR OF PHILOSOPHY

May 2011

Major Subject: Chemistry

Simple Chemical Routes for Changing Composition or Morphology in Metal Chalcogenide Nanomaterials

SIMPLE CHEMICAL ROUTES FOR CHANGING COMPOSITION OR MORPHOLOGY

IN METAL CHALCOGENIDE NANOMATERIALS

A Dissertation

by

STACEY ELAINE WARK

Submitted to the Office of Graduate Studies of
Texas A&M University
in partial fulfillment of the requirements for the degree of

DOCTOR OF PHILOSOPHY

Approved by:

Chair of Committee,	Dong Hee Son
Committee Members,	James D. Batteas
	Simon W. North
	Daniel F. Shantz
Head of Department,	David H. Russell

May 2011

Major Subject: Chemistry

ABSTRACT

Simple Chemical Routes for Changing Composition or Morphology in Metal Chalcogenide Nanomaterials. (May 2011)

Stacey Elaine Wark, B.S., University of Dallas

Chair of Advisory Committee: Dr. Dong Hee Son

Metal chalcogenide nanomaterials are interesting due to their size dependent properties and potential use in numerous types of devices or applications. The synthetic methods of binary phase metal chalcogenide nanoparticles are well established, but finding simple ways to make even more complex nanostructures is important. To this end, two techniques were studied: the cation exchange of metal chalcogenide nanocrystals, $CdE \rightarrow M_xE_y$ (E = S, Se, Te; M = Pd, Pt) and the solution phase synthesis of ternary chalcogenide nanoparticles.

The effects of cation solvation and the volume change (ΔV) of reaction on the equilibrium and the morphology change in the cation-exchange reactions of $CdE \rightarrow M_xE_y$ were investigated. A two-phase solvent environment was particularly efficient in increasing the thermodynamic driving force. The effect of ΔV of reaction on the morphology of the product nanocrystals was also investigated. Depending on the stress developed in the lattice during the reaction, product nanocrystals underwent varying degrees of morphological changes, such as void formation and fragmentation, in addition to the preservation of the original morphology of the

reactant nanocrystals. The knowledge of the effect of ion solvation and ΔV of reaction on the equilibrium and product morphology provides a new strategy and useful guide to the application of cation-exchange reactions for the synthesis of a broader range of inorganic nanocrystals.

Using a solution phase method, the morphology of $CuInSe_2$ nanoparticles could be tuned from small 10 nm spheres to micron length nanowires by varying the relative amount of strong and weak surfactants passivating the surface. Oleylamine and trioctylphosphine oxide were chosen as the strong and weak surfactants, respectively. Small isotropic structures were formed when the oleylamine was the only surfactant with the size of the nanospheres increasing as the amount of oleylamine decreased. For the $CuInSe_2$ nanowires, weakly-binding dioctylphosphine oxide (DOPO), an impurity in the TOPO, was found to be the key surfactant that enables the anisotropic one-dimensional growth. Detailed analysis of the structure of the nanowires indicated that they grow perpendicular to (112) planes, with twinning around the growth axis by ~60° rotation. The nanowires exhibit a saw-tooth surface morphology resembling a stack of truncated tetrahedral.

DEDICATION

To Mom, Dad and Shelly

I love you.

ACKNOWLEDGMENTS

First and foremost I must give thanks to God for the many gifts and opportunities he has given me. I could not have gotten through this process without my faith and trust in Him. Earning my Ph.D. has been a very humbling yet amazing experience. The amount of support and encouragement that I have received has truly astonished me and it has made me realize how truly blessed I am.

Thank you to my advisor, Dong Hee Son, for being patient and working with me, even when things did not look hopeful. In addition, thank you to my committee members, James Batteas, Simon North and Daniel Shantz, for their help and guidance. To Dr. Zhiping Luo from the MIC at Texas A&M University, thank you for your help and collaborations over the years. Your expertise and enthusiasm about electronic microscopy was contagious and you were an amazing teacher.

To current and previous members of the Son group, thank you! To Chih-Hao and Tai-Yen especially, thank you for your friendship and camaraderie these last 5 plus years. To Chih-Hao, thank you for always being upbeat and fun to work with. Tai-yen, you were an amazing scientific role model with your level head, guidance and leadership in the Son group. Thank you for you for the help in understanding how to think about scientific problems.

To my extended family, (my grandparents and many aunts, uncles and cousins), thank you for the cards, texts, words of encouragement and overall

support you have given me. You are a stabilizing force in my life and such a blessing. To all of my friends, thank you for hanging in there with me the last six years, especially Tamsin and Veronica. Both of you always knew what to say and your support has been amazing. I look forward to many more years of friendship with both of you.

Words cannot express my gratitude for the unconditional love and unwavering support I have received from my mom, dad and sister–I love you! Mom and Dad, thank you for instilling in me the value of an education. Your willingness to help me through all of the tough times in grade school all the way through graduate school have allowed me to come this far. Please know that the many sacrifices you made to give me the best education possible have not gone unnoticed–thank you! Mom, thank you for the countless loads of laundry and the many wonderful meals you made for me. Your generosity always amazes me! Dad, I think I inherited your curiosity, and it is one of the best gifts you could have given me. Thanks to both of you for instilling in me a work ethic to provide for myself while still being able to kick back and enjoy life.

Shelly, I have looked up to you for longer than I can remember and you have been an amazing role model. Thank you for always believing in me, even when I doubted in myself. The many late night phone calls, trips to Waco and encouragement you have provided have kept me sane for the last six years. Thank you for always being interested in my research (even if you were just pretending). I

am truly fortunate to be able to call you not only my sister but one of my best friends.

"Appreciate" does not even begin to cover or describe how I feel about each and every person involved in this project. I cannot believe this journey is over, and I will never forget all the people who help get me to this wonderful destination. Thank you so much!

TABLE OF CONTENTS

CHAPTER Page

Page

LIST OF FIGURES

FIGURE Page

FIGURE Page

FIGURE Page

LIST OF TABLES

CHAPTER I

INTRODUCTION

1.1 General background

Metal chalcogenide nanomaterials have interesting properties that differ from their bulk counterparts. These properties depend not only on the material of the nanoparticle but also on the size and shape of the particle as well. Spherical semiconducting metal chalcogenide nanoparticles have tunable band gaps that are dependent on the radius of the nanoparticle due to quantum confinement effects.[1] Semiconducting nanorods have tunable band gaps as well, but the band gap depends more strongly on the diameter of the rod than on the length. Emission polarization is an example of a property in nanoparticles that is dependent on shape, where the emission of spherical particles is depolarized, but the emission of nanorods is linearly polarized.[2] In addition, the chemical and physical properties of nanoparticles can differ from their bulk counterparts as well. For example, nanoparticles have a lower melting point than their bulk counterparts which can be explained by the high surface to interior ratio of atoms in a nanoparticle.[3]

The synthetic methods of simple morphologies such as spheres, cubes and rods/wires of binary phase metal chalcogenide nanoparticles have been well studied.[4-9] Binary metal chalcogenide nanoparticles have shown potential in

---

This dissertation follows the style of *ACS Nano.*

possible application such as emitting diodes, solar cells or lasers.[1] Making more complex nanostructures is the next step for nanoparticle synthesis. Specifically, developing simple ways to make complex nanoparticles or modifying existing nanoparticles (which already have a well developed synthetic method) may allow nanoparticles to be more accessible for use in applications.

More complex nanostructures are desired for several reasons. The first reason would be to have a single nanostructure with two different materials that retain the individual properties. An example of this complex structure is having both a semiconducting and a magnetic domain. This type of structure may be useful in dual functional molecular imaging.[10] The second reason to have a complex nanostructure would be a single nanostructure in which the properties of one of the materials strongly affect the properties of the other material. This type of structure has been seen in type-II core/shell heterostructures. For example, CdTe/CdSe core/shell structures emit in the near-IR region, which is not accessible by either CdSe or CdTe nanoparticle by themselves.[11] Knowing that complex nanostructures can have advantages over simpler nanoparticles, the goal is to find simple ways to make complex nanostructures.

Nanoparticles, whether simple or complex, can be made from either a top down or bottoms up approach. Top down approaches take larger structures and make them smaller, such as ball milling and laser ablation,[12-14] but these methods have several drawbacks that include trouble controlling shape or size distribution and not being able to make very small particles. Bottoms up approaches use atoms

or molecules to make larger structures and are better suited to make uniform nanostructures over the top down approaches. Bottoms up methods include liquid or vapor phase epitaxy, template systems or colloidal methods.[15] Colloidal methods, or solution phase syntheses, have shown a high degree of control over the size and shape of semiconducting, metal and metal oxide nanoparticles. This control is achieved through regulation of thermodynamic parameters and growth kinetics through the assistance of selected solvents, ligands, surfactants or catalysts.[16] Solution phase synthesis must precisely control multiple variables such as temperature variation, choice of precursor, precursor concentration and solvent and surfactant purity to obtain the desired morphology or size.

Solution phase growth of complex nanostructures has been studied in numerous different systems with components such as semiconductors, metal oxides and metals.[17-28] Heterostructures can be made in numerous different ways such as direct heterogeneous deposition, redox reactions, thermally induced phase segregation, solid-state diffusion or ion exchange.[16] The interface between the different materials in the structure is just one of the considerations for solution phase synthesis techniques. For materials with similar lattice constants, epitaxial growth is expected and, as an example, core/shell structures can be made.[29] When the lattice mismatch is large, the resulting nanostructure can be harder to predict. For example, noncentrosymmetric structures of γFe_2O_3 with MS (M = Zn, Cd, Hg) were formed when large lattice mismatch is present.[21] As the lattice mismatch increased, structures went from multijunction particles to dimmers then to

completely separate particles with a few dimmers. In addition, a challenge of solution phase synthesis is controlling the position of the different components in complex nanostructures. For example, random nucleation of the second material or the incorporation of mixed phases of materials are examples of why control is limited for heterostructures.[19]

The previous materials discussed have been either binary or single element nanoparticles (or domains in nanoparticles). Ternary or quaternary nanostructures, with three or four elements respectively, are another example of nanoparticles which are interesting. For example, I-III-VI_2 materials such as $CuInSe_2$ have high optical absorption coefficients and are stable in the sun's radiation, which make them promising candidates for solar cell applications.[30] In addition, ternary (and quaternary) systems have much more tolerance in the elemental composition of a given crystal phase, which can affect their material properties such as ban gap. In $CuInSe_2$ thin films, as the ratio of Cu/In increases the band gap blue shifts.[31] Another type of ternary material is an alloy (or solid solution) such as $PbSe_yS_{1-y}$[32] or $CdSe_xTe_{1-x}$.[32, 33] The ternary alloys have shown promise because it allows for modification of properties based on composition, not just size. In semiconducting nanoparticles of binary material, properties (e.g. electronic or optical) are varied by changing the size of the nanoparticles; however, in ternary alloys, it has been shown that by varying the ratio of Se to Te in $CdSe_xTe_{1-x}$ alloy nanoparticles, the optical and electronic properties could be tuned (while keeping size constant).[33]

Solution phase synthesis of ternary chalcogenide nanoparticles has unique challenges as compared to binary chalcogenide nanoparticles. One of the main challenges is the reaction of three or more different elemental precursors forming the desired crystal structure.[34] Balancing the decomposition temperatures or ligand binding affinities of three or more elemental precursors are examples of why the elemental composition of the nanoparticle can vary and be difficult to control. The previous problem, coupled with shape and size control in the nanoscale region, is why the synthetic methods of ternary or quaternary phases are not as developed as binary systems.[34]

1.2 Simple routes for changing composition or morphology in nanomaterials

Understanding the problems that are encountered in the synthesis of complex nanostructures (whether in composition or morphology) makes one understand why finding simple ways to make complex nanostructures is of importance. Conversion chemistry is an example of a simple technique to modify composition or morphology in nanoparticles in which new and more complex nanostructures can be made. Conversion chemistry uses a starting nanoparticle as a template and transforms it into a chemically different species through the use of ion exchange, diffusion, oxidation, galvanic replacement, etc.[34]

Diffusion and exchange of atoms in nanoparticles have been seen in many systems and are a useful way to modify composition.[34-38] The kinetics of a cation exchange reaction (CdSe going to Ag_2Se) was found to be much different in

nanomaterials than in bulk due to high collision efficiency values and low activation energy.[39] Cation exchange has been shown to be useful in the conversion of both nano and mesoscale systems and are able to form more complex structures such as heterostructres or periodic superlattices.[35, 38, 40, 41]

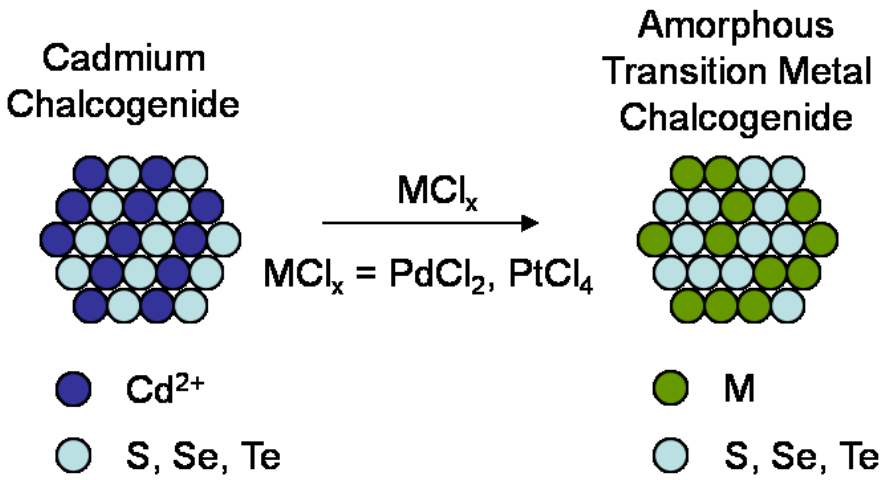

Figure 1.1. General scheme of the cation exchange reaction for $CdE \rightarrow M_xE_y$, (E=S, Se, Te and M=Pd, Pt). The resulting nanoparticles after the cation exchange are amorphous.

Due to the usefulness and versatility of the cation exchange reactions in nanoparticles, a better understanding is needed of how certain parameters can be changed and varied to make the desired nanoparticles. The aim of the first part of this dissertation is to gain more information about several reaction parameters in cation exchange reactions. Solvation conditions and volume change of reaction

were the chosen parameters because solvation studies may allow for the possible tailoring and manipulation of the thermodynamics of the ion exchange reaction, and the volume change of reaction allows insight into morphology conservation or lack thereof. The goal of studying the cation exchange reaction is to establish a framework which would allow the cation exchange reaction to be used in numerous other systems.

Figure 1.1 illustrates a general scheme of the system of interest, starting with nanoparticles of cadmium chalcogenide (S, Se or Te), which undergo a cation exchange with either platinum or palladium cations. Both platinum and palladium have a wide variety of stoichiometry with the chalcogenides that can be formed. Platinum and palladium chalcogenides were studied because of their possible applications in catalysis or in the semiconductor or electronics industry.[42]

The second project of this dissertation covers the development of a solution phase synthesis of ternary chalcogenide nanoparticles. While the solution phase synthetic methods of binary chalcogenide nanomaterials (such as CdSe) are well understood, ternary chalcogenide are more difficult to make due to the complexity of the phase diagram and reaction kinetics of the multi-component system. $CuInSe_2$ was used as a model system because of its potential uses in photovoltaic or thermoelectric devices.[43-45] There have been numerous reports on the solution phase synthesis of $CuInSe_2$ nanoparticles which yield a variety of different morphologies and sizes. Within these reports, though, is a lack of understanding of how different synthetic variables affect the resulting morphology or size of the

nanoparticle. To this end, the purpose of the second project was to gain insight into how surfactants specifically played a role in the morphology and size of ternary chalcogenide nanoparticles. The goal would be to utilize this understanding which would allow a simple way in which one could tune the morphology of ternary semiconducting nanomaterials.

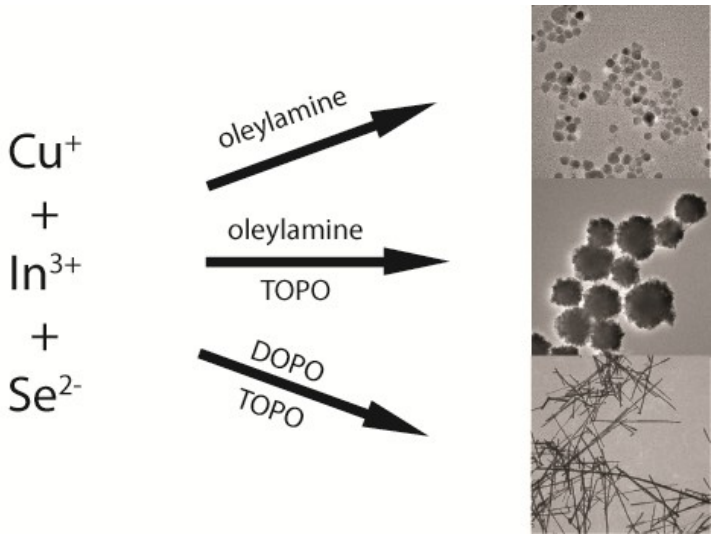

Figure 1.2. General scheme of the different morphologies of $CuInSe_2$ produced in solution phase. The surfactants used are shown above/below the respective arrows for each morphology. The sizes of the nanoparticles from top to bottom are ~10 nm (top), ~250 nm (middle) and ~60 nm in diameter and microns in length (bottom).

It was hypothesized that by changing the binding affinity of the surfactants used, the morphology could be systematically varied. Oleylamine and trioctylphosphine oxide (TOPO) were chosen as the strong and weak binding surfactants, respectively. When a strongly binding surfactant was used, small isotropic nanoparticles were formed, but when a weak binding surfactant was used, larger anisotropic shapes were formed. When a combination of the two surfactants was used, large isotropic nanoparticles were formed. Dioctylphosphine (DOPO), an impurity found in TOPO, was found to be the key surfactant to make anisotropic nanowires. Figure 1.2 shows the general scheme employed to make different morphologies of $CuInSe_2$.

To understand the role of the surfactant in the growth of anisotropic particles, the nanowires were characterized at different times in the synthesis. It was found that the nanowires had rough surfaces and grew by a continuous growth mechanism. In addition the wires were polycrystalline and grew perpendicular to (112) plane. Twinning occurred in the nanowires with a rotation around the growth axis of ~60°.

1.3 Thesis overview

In the following chapters, the two experiments are explained in detail. The background and principles of cation exchange in nanoparticles will be discussed in Chapter II, and it will go into an in-depth discussion on cation exchange specifically showing the usefulness of cation exchange as a simple way to modify composition

in nanoparticles. Chapter III follows explaining experimental details of the cation exchange system showing the results along with the conclusions drawn from them. Chapter IV will introduce surfactant direct morphology control and the issues for making ternary chalcogenide nanomaterials in solution phase synthesis. Chapter V includes the experimental data and the conclusions from the solution phase synthesis of $CuInSe_2$ nanoparticles with Chapter VI concluding the thesis.

CHAPTER II

THE USE OF CATION EXCHANGE IN NANOPARTICLES

2.1. Conversion chemistry in nanomaterials

Modification of nanoparticles which have a well developed synthetic method is a simple way to make more complex nanostructures. "Nanocrystal conversion chemistry" was a term coined by Schaak's group that encompasses solution based chemistry which takes a starting nanoparticle and chemically transforms it into something else.[34, 41] Numerous groups have studied methods for the transformation of nanomaterials, which include galvanic replacement, oxidation, diffusion and ion exchange.[35, 46-49] Depending on the specific reaction conditions used, morphology may or may not be conserved.[50] The ultimate goal would be to understand fully all types of transformations in the conversion chemistry of nanoparticles to give scientists a "tool box" for which the production of complex nanostructures that have the desired characteristics for potential applications becomes possible.[34]

Conversion chemistry uses nanoparticles with well established synthetic procedures as reactive temples which can be partially or completely transformed. Complete conversions, in regards to composition, can be useful to make nanomaterials for which no synthetic methods are available. For example, Pt_3Te_3 nanoparticles were formed through a galvanic replacement between tellurium nanowires and a platinum chloride salt. The authors state that this was the first report of the synthesis Pt_3Te_3 nanomaterials.[50] Metal nanoparticles could be turned

into metal phosphide nanoparticles with the use of phosphines, such as trioctylphosphine. This is an example where a whole class of compounds which could be accessed due to diffusion.[46, 51-54]

In respect to morphology, conversions, whether partial or complete, can lead to a variety of complex nanostructures such as core/shell, tipped nanorods or wires, or hollow nanoparticles. For example, hollow cobalt sulfide nanoparticles were formed by taking cobalt nanoparticles and reacting them with sulfur in dichlorobenzene. The void in the nanoparticle was formed due to differing diffusion rate of the sulfur diffusing into the nanoparticle and the cobal diffusing out (a Kirkendall-like mechanism).[48] Core/shell structures could be made using cation exchange to make CdSe/Ag_2Se nanoparticles.[55] Using galvanic reduction reactions, silver tipped ZnO nanorod arrays could be formed.[56]

Conversion chemistry is not restricted to only the nanoscale regime. Xia and coworkers make large mesoscale heterostructures of Se:Ag_2Se by starting with Se spheres of between 100 to 400 nm which were then reacted with Ag. The Se:Ag_2Se particles could then undergo a subsequent cation exchange to form Se:MSe (M=Zn, Cd or Pb).[41, 57] These previous examples show the versatility of nanoconversion chemistry.

2.2 Ion exchange in nanoparticles

Chemical modification of nanocrystalline solids via diffusion or exchange of atoms has been recently demonstrated to be a simple and versatile way to create a

variety of inorganic nanostructures.[35, 41, 47, 49, 57-59] Cation exchange reaction in ionic nanocrystals, in particular, has been shown to be very useful for transforming ionic nanocrystals into other ionic nanocrystals, hetero-interfaced and periodic superlattice nanostructures.[35, 38, 57]

Cation exchange had been extensively studied in thin films before it was applied to nanoparticles.[60, 61] Cation exchange in thin film showed that the technique was advantageous because it was an economical and easy way to make Ag_2S thin films as compared to a direct chemical deposition method. In addition, the thin films made by the cation exchange method had more desirable properties (e.g. lower resistivity). After cation exchange, the crystal domains were ten times smaller than the starting material (CdSe or CdS which had 2 to 3 micron domains), and the exchange took anywhere from 15 minutes for CdS to Ag_2S to 90 minutes for CdSe to Ag_2Se.[60]

Son and coworkers studied the same cation exchange reaction of CdSe with Ag^+ except in nanoparticles.[35] It was found to be a fast and efficient way to modify composition with the reaction taking less than 1 second.[35] The crystal structure of the reactant and product were similar and the reverse reaction of Ag_2Se to CdSe could be achieved by the addition of tributylphosphine (TBP). TBP forms an intermediate complex with the Ag and, with the addition of gross excess of Cd^{2+}, forces the reverse reaction at slightly elevated temperatures. Only with the addition of TBP will the reverse reaction proceed. In this example of cation exchange, the ions were solvated in methanol, which was about 1% by volume of

the total solution. Due to the speed and reversibility of this reaction, the activation barrier is thought to be rather small, and such fast kinetics and reversibility of the reaction are considered mainly due to the lower activation barrier for the diffusion of atoms in nanocrystalline solids. This example shows how the fundamental kinetics of nanoparticles are drastically different than the bulk phase and even differ from thin films as well.[39]

Other cation exchanges have been seen, such as ZnS with Cu^{+}, Ag^{+}, Sb^{3+} and Bi^{3+}.[59] In this case of cation exchange, cations along with the starting reactants are solvated in water. The solubility of the products formed was less than the reactants, and the authors stated that this condition must be met for cation exchange to take place. For reactions in which the solubility of the products is not less than the reactants, some reaction condition needs to be changed to make the reaction proceed, such as the addition of TBP.

Cation exchange was extended to mesoscale systems by Xia, et al. Se@Ag_2Se spheres were made, which can then be subsequently converted to Se@MSe (M = Zn, Cd, Pb) with size and shape conversion.[41, 57] The exchange reaction is performed in only methanol. The TBP is known to bind with metal ions, but due to the stronger interaction of TBP with Ag, the Zn, Cd, or Pb are left to exchange. All of these exchanges were carried out at about 50°C. The authors comment that the use of only methanol is needed for the reaction to take place and theorizes that the methanol may act as a ligand along with the TBP.

For reactions that are not spontaneous, ligands, such as TBP, have been used to complex with metal as seen in the reaction of Ag_2Se to CdSe. The important idea here is the ability to change the solubility of both cations, in the reactant and product. In the previous examples of cation exchange, the solvent environment has not been investigated to see what role it plays in the overall thermodynamic and kinetics of the reactions. Understanding how solvent conditions along with ion solubility affects ion exchange reactions will allow for better control and tailoring of reaction conditions. Solvation studies will allow for possible tailoring of the thermodynamics of the ion exchange reactions.

The previous discussion has been focused on solvation conditions, and the use of complexing agents to allow the reverse cation exchange reaction to take place. The crystal structure of the reactant and product nanoparticle also needs to be discussed. An easy way to quantify the change of crystal structure is to calculate the volume change of the unit cell from reactant to product, denoted by $\Delta V/V$. In the previous cation exchanges discussed (of CdSe to Ag_2Se and Ag_2Se to ZnSe, CdSe and PbSe), the $\Delta V/V$ has been around 0.05 or 5%. This $\Delta V/V$ is a relatively small change, and the morphology or the nanoparticle is typically conserved. In order to expand the use of cation exchange reactions to other systems, where $\Delta V/V$ may be much larger, more insight into how $\Delta V/V$ affects the resulting morphology of the nanoparticles is needed.

Anion exchange has proven more difficult in solution phase. This may be due to the large size of the cation, but is more likely due to the stable anion

framework in ionic nanocrystals, specifically in transition metal chalcogenides. It was found that the anionic framework was conserved during cation exchange with the use of a CdSe/CdS nanorods.[37] More complex starting heterostructures may now be utilized in cation exchange reaction knowing that the anionic framework of ionic nanocrystals is stable. That being said, anion exchange has been seen before in a handful of systems, but typically the reaction conditions are harsher than those of cation exchange reactions.[59, 62, 63] For example, a ZnO columnar film was transformed into ZnS by the use of H_2S gas at around 500°C.[59]

In principle, the high efficiency of the cation exchange reaction in nanocrystals can be extended more broadly to the exchange reactions with other cations or possibly even anions.[64] Ultimately, the efficiency of the cation exchange reaction as a synthetic method will depend on the thermodynamic driving force and the activation barrier. In order to utilize the cation exchange reaction as a versatile synthetic method of nanocrystals, it will be important to understand and perhaps control the factors affecting the kinetics and thermodynamics of the reaction other than temperature and concentration. Since the net reaction involves the exchange of two cations, solvation of cations is an important factor determining the thermodynamics of the reaction. Cation solvation can be controlled to a certain extent by varying the solvent environment, which will influence the overall thermodynamics of the reaction. In the simplest case, one could vary the solvation condition by changing the polarity of the solvent.

Consideration of the factors affecting the activation barrier is slightly more complicated. The activation barrier for the diffusion and exchange of the cations will depend on many factors such as the structure of anion sublattice, ionicity of cation-anion interaction, structural difference between the reactant and product phases, etc. Among these factors, the structural difference between reactant and product phases is a more easily quantifiable factor and bears additional importance concerning the morphology change of the nanocrystals after the reaction. Morphology change of the nanocrystals, especially when the reaction accompanies a large change in the volume or lattice parameters, can be an important issue when the initial reactant nanocrystals are used as the structural template.[35, 52, 59]

In this work, the effect of solvent environment on the equilibrium and efficiency of the cation exchange reaction was studied as well as the effect of volume change of the reaction on the morphology change in the product nanocrystals. The studied cation exchange reactions are $CdE \rightarrow M_xE_y$, (E=S, Se, Te and M=Pd, Pt) occurring under ambient conditions, illustrated in Figure 2.1. The fractional volume change ($\Delta V/V$) of reaction ranges from -0.25 to -0.46, based on bulk lattice parameters.[65-69] For all the reactions studied, the equilibrium of the reaction was strongly dependent on the variation of the solvent environment, which modified the thermodynamics of the reaction by changing the cation solvation condition. In particular, a two-phase solvent environment, where the two cations involved in the exchange reaction were separated in different phases, strongly favored the forward reaction. This experimental evidence clearly indicates

the importance of the cation solvation by solvent medium in determining the thermodynamic driving force and therefore the efficiency of the reaction. While all the reactions were slower than the case of CdSe $\rightarrow$ Ag_2Se, the activation barrier was still sufficiently low for the reaction to occur even at ambient temperature. These results suggest the possibility of applying various selective cation complexing reagents, more commonly used in organic reactions (e.g. crown ether), to enhance the efficiency of the ion exchange reactions of nanocrystals. Relatively large $\Delta V/V$ of the reaction had varying degrees of effects on the morphology of the product nanocrystals. Void formation and fragmentation, as well as the preservation of the original morphology, were observed depending on the degree of lattice stress in the product nanocrystals developed during the reaction. The platinum and palladium chalcogenide nanoparticles made by cation exchange showed little crystallinity. They were amorphous and with heating could be crystallized into the most thermodynamic phases. Both in-situ and ex-situ experiments were performed.

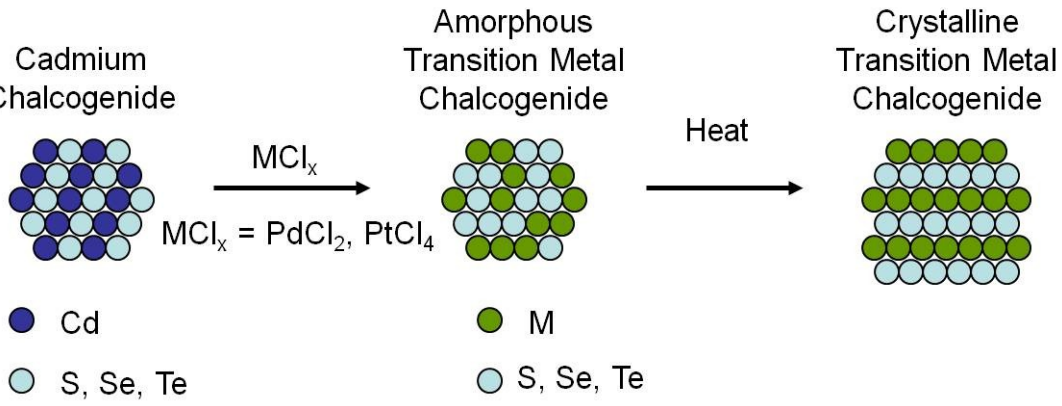

Figure 2.1. General scheme of cadmium chalcogenide nanoparticles undergoing cation exchange to form an amorphous platinum or palladium chalcogenide. After heating, the amorphous transition metal chalcogenide crystallizes into the most thermodynamically stable phase with no morphology conservation.

CHAPTER III

THE EFFECT OF ION SOLVATION AND VOLUME CHANGE OF REACTION ON THE EQUILIBRIUM OF CATION EXCHANGE IN NANOPARTICLES*

3.1 Experimental section

3.1.1 Materials

The following chemicals were purchased from Aldrich and used without further purification: Trioctylphosphine Oxide (TOPO 99%), palladium (II) chloride ($PdCl_2$, 99%), Platinum (IV) Chloride ($PtCl_4$, 98%,) hexadecylamine, cadmium oxide, sulfer, selenium, tellurium, tributyl phosphine, octadecene, oleic acide, octanonic acid and didodecyldiethylammonium bromide. Tetradecylphosphonic acid and hexylphosphonic acid was purchased from Polycarbon Industires, Inc.

3.1.2 Synthesis of cadmium chalcogenide nanoparticles

Spherical nanocrystals of CdS, CdSe and CdTe were synthesized following the well-established solvothermal methods using CdO and elemental S, Se and Te dissolved in coordinating solvents as precursors.[7, 70, 71] Standard airless procedures were used for all nanoparticle synthesis. Figure 3.1 illustrates the typical

* Reprinted in part with permission from *J. Am. Chem. Soc*. Wark, S. E.; Hsia, C. H.; Son, D. H., Effects of ion solvation and volume change of reaction on the equilibrium and morphology in cation-exchange reaction of nanocrystals. *J. Am. Chem. Soc.* **2008,** *130* (29), 9550-9555

experimental setup used to synthesis the cadmium chalcogenide nanoparticles.

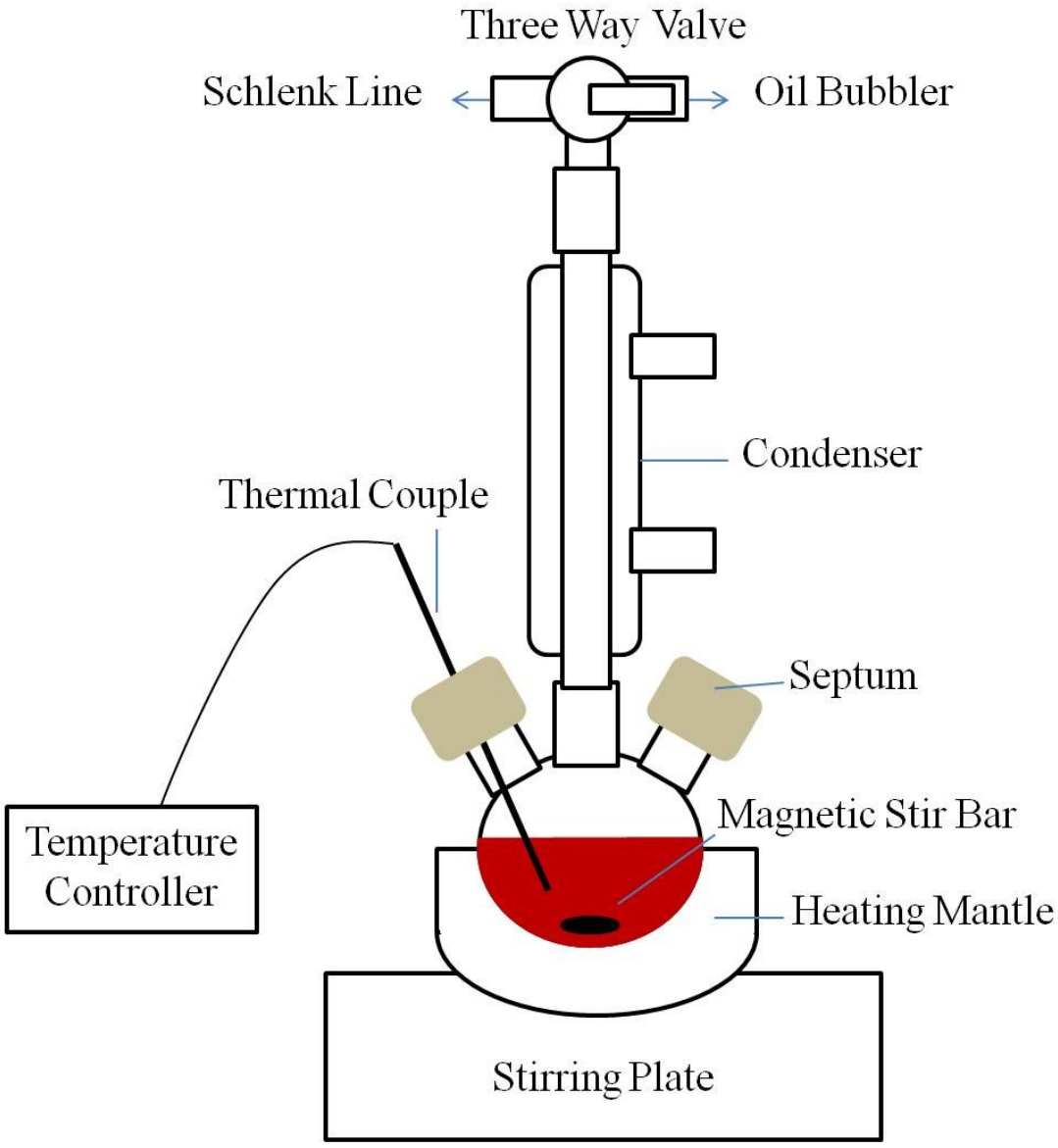

Figure 3.1. Schematic diagram of the experimental set up for the synthesis of cadmium chalcogenide nanoparticles.

CdSe nanoparticles were made using 0.012 mole (2.85 g) of hexadecylamine, 0.003 mole (1.15 g) of trioctylphosphine oxide, 0.004 mole (1.09 g) of tetradecylphosphonic acid and 0.002 mole (0.250 g) of cadmium oxide which were added into a three neck round bottom flask and heated under vacuum at 100-110 °C for I hour. The flask was then backfilled with nitrogen and heated to 300 °C until the solution turned optically clear and 0.5 g TBP was injected. The temperature was then lowered to 270 °C and an 0.8 gram solution of Se:TBP (10% by weight, .001 mole of Se) was swiftly injected. The reaction was monitored by UV-Vis and the reaction was stopped when the desired size was made. The reaction flask was quickly cooled by blowing N_2 around the bottom of the flask. When the solution reached 60 °C, 10 g of octanonic acid was added to prevent the formation of a gel. Methanol was then added until the solution was turbid. The solution was then centrifuged and the supernatant was discarded. The supernatant should have a slight yellow color from the octanonic acid, and the precipitate should be highly colored. If a considerable amount of precipitate is observed, then you still have a gel and it should be redisolved in toluene and octanonic acid. Once the supernatant is discarded the precipitate should be dissolved in toluene and reprecipitated with methanol.

CdS nanospheres were made using 0.5 mmole (0.064 g) CdO in 21.75 ml ODE and 3.2 ml oleic acid which were added into a three neck round bottom flask and heated under vacuum at 100-110 °C for I hour. This solution was heated under N_2 to 300 °C until the solution turned optically clear. The solution was cooled to

270 °C and 6.25 ml of S:ODE (0.625 mmole, 0.02 g of sulfur in 6.25 ml of ODE) was swiftly injected. The growth temperature was held at 250 °C. The reaction was monitored by UV-Vis and the reaction was stopped when the desired size was made. The reaction flask was quickly cooled by blowing N_2 around the bottom of the flask. The reaction solution was cleaned with a dichloromethane:methanol (1:1) extraction. The particles (which were in the dichloromethane layer were then precipitated by adding acetone. The precipitate was redissolved in toluene. Two more cleaning were done using methanol to precipitate and toluene to dissolve the CdS nanoparticles.

CdTe nanospheres were made using 0.001 mole (0.13 g) of cadmium oxide in 0.007 mole (1.95 g) TDPA and 0.017 mole (6.38 g) TOPO which were added into a three neck round bottom flask and heated under vacuum at 100-110 °C for I hour. The flask was then backfilled with nitrogen and heated to 300 °C until the solution turned optically clear. The solution was then cooled to 270 °C and 2 g of Te:TOP (10% by weight, 0.002 mole Te) was swiftly injected. The reaction was monitored by UV-Vis and the reaction was stopped when the desired size was made. The reaction flask was quickly cooled by blowing N_2 around the bottom of the flask. When the solution reached 60 °C, 10 g of toluene was added. Methanol was then added until the solution was turbid. The solution was then centrifuged and the supernatant was discarded. The precipitate was then redissolved in toluene and cleaned twice more using methanol to precipitate and toluene to dissolve the CdTe nanoparticles.

CdSe nanorods were synthesized following the procedure developed by Peng et al.[9] 0.105 grams of cadmium oxide was mixed together with 0.39 grams of tetradecylphosphonic acid, 0.08 grams hexylphosphonic acid and 1.425 grams of trioctylphosphine oxide in a three neck round bottom flask. The flask was then heated under vacuum at 100-110 °C for 30 minutes. The flask was then backfilled with nitrogen and then heated to 300 °C until the solution turned optically clear. Once the solution became clear, the heat was removed and the flask was then left at room temperature for 24 hours under the nitrogen flow. After aging the solution, the flask was then heated to 300 °C again until the mixture had dissolved. The heat was lowered to 250 °C and 1.6 g of a 4% by weight solution of Se:TOP was swiftly injected. The reaction was monitored by UV-Vis and the reaction was stopped when the desired size was made. The reaction flask was quickly cooled by blowing N_2 around the bottom of the flask. When the solution reached 60 °C, 10 g of toluene was added. Methanol was then added to the solution until turbid and then the solution is centrifuged. Both the nanorods and spheres were cleaned using repeated precipitation by using methanol and redisolving the nanoparticles in toluene. The nanoparticles were cleaned at least three times.

3.1.3 Cation exchange procedure

All the nanocrystals used in the cation exchange reactions were dispersed in toluene. For the cation exchange reaction, $PdCl_2$ and $PtCl_4$ were used as the source of cations. Three different reaction conditions that provided different cation

solvation environment were used as described in Table 3.1. The reactions occurred in a single-phase solvent environment under condition (A) and (B), and in a two-phase solvent environment under condition (C). Didodecyldiethylammonium bromide (DDAB) used in condition (B) and (C) provided the metal salts solubility in toluene, probably by forming a DDAB-metal chloride complex.[72] In a simple extraction experiment, approximately one equivalent of DDAB was needed to extract one equivalent of metal ion from aqueous phase to organic phase. Typical concentrations of the nanocrystals (CdE formula unit base) and metal salts (MCl_n) in the final reaction mixture were approximately 0.1 mM and 5 mM respectively.

$PdCl_2$ has limited solubility in methanol. To make the $PdCl_2$ methanolic solution, an excess of palladium salt (200 mg) was added to 3 ml of methanol. This solution was sonicated for about 1 hour and then centrifuged. The supernatant could then be used for the cation exchange procedure on that day. The solution could not be used after a few days because the palladium could be reduced by the methanol. A similar procedure was used for the $PtCl_4$ methanolic solution with $PtCl_4$ being more soluble than the palladium salt in methanol. 350 mg of $PtCl_4$ was added to 3 ml of methanol and sonicated for 15 minutes. The solution was the centrifuged and the supernatant could then be used for the cation exchange procedure for that day. The platinum solution, just like the palladium solution, could reduce the platinum to the metallic form.

Table 3.1. Reaction conditions and solvent environments for cation exchange reaction between cadmium chalcogenide nanocrystals (CdE) and metal chloride (MCl_n).

	(A)	(B)	(C)
Reaction Conditions	CdE (toluene, 2.5 ml) + MCl_n (methanol, 0.5 ml)	CdE (toluene, 0.10 ml) + MCl_n (toluene, DDAB, 1.9 ml)	CdE (toluene, DDAB, 2 ml) + MCl_n (water, 1 ml)

All the reactions were performed by mixing the nanocrystal solution with the metal salt solution under ambient condition. The reaction time was varied from a few minutes to several hours depending on the detailed reaction condition. After the reaction, the product nanocrystals were precipitated by adding methanol and centrifuging the reaction mixture. The recovered nanocrystals were rinsed with methanol for further characterization of the structure and composition.

The platinum and palladium chalcogenide nanoparticles were amorphous after exchange. Both in-situ and ex-situ heating experiments were preformed on PdSe to observe how the nanoparticles would crystallize. In addition, ex-situ experiments were performed on all the rest of the platinum and palladium chalcogenides. The in-situ experiment was performed on a TEM grid which had a Si_3N_4 window. This type of grid was used to withstand the heat and not degrade under the high heat. A heating stage was used to control the temperature. For the ex-situ heating experiment of the PdSe, 0.1 mmol of PdSe was added to 5 ml ODE and heated to 200°C for 20 minutes. For the other platinum and palladium chalcogenides, the nanoparticles were heated on a glass slide open to the air for 5 minutes. A solution of the nanoparticles was drop cast onto the glass slide and the color of the thin film was observed to change from a brownish to black.

3.1.4 Characterization of nanoparticles

The lattice structures of the reactant and product nanocrystals were examined by taking powder x-ray diffraction (XRD) patterns of the dried samples

on a Bruker-AXS GADDS diffractometer. Transmission electron micrographs (TEM) of the nanocrystals were acquired using a JEOL 2010 transmission electron microscope. For in-situ study of the structure of the thermally annealed nanocrystals, TEM and electron diffraction patterns of the nanocrystal samples on Si_3N_4 substrate were recorded before and after the heating. Elemental composition of the nanocrystals was obtained from energy dispersive x-ray (EDX) analysis employing Oxford Instruments INCA EDX system. Oxidation state of Pd and Pt cations in the product phase was determined from x-ray photoelectron spectroscopy (Kratos Axis Ultra).

3.2. Results and discussion

3.2.1 Effect of solvent on the equilibrium

In order to investigate the effect of cation solvation condition on the equilibrium of the cation exchange reaction, three different reaction conditions were used as described in Table 3.1. Under condition (A), metal cations were solvated by a small amount of methanol homogeneously mixed with toluene. The same condition was used for the reaction CdSe $\rightarrow$ Ag_2Se in earlier studies.[35, 38] Under condition (B), both metal cations and reactant nanocrystals were in the toluene phase. Under condition (C), Pd and Pt cations were initially in the aqueous phase. During the reaction, DDAB transported Pd and Pt cations into toluene phase, while the exchanged Cd cations were solvated in the aqueous phase.

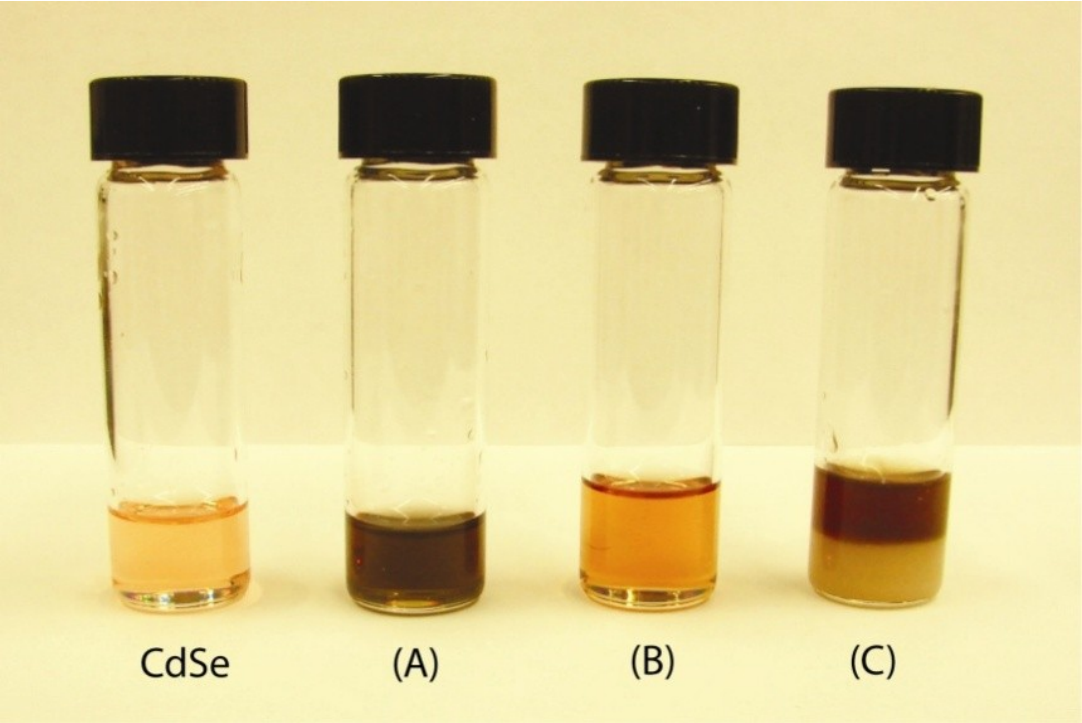

Figure 3.2. Photographs of the reaction mixtures under the condition (A)-(C) described in Table 1. The starting CdSe nanoparticles are shown as a reference.

When comparable total concentrations of the reactants were used, cation exchange was the most efficient under condition (C), followed by condition (A) and (B) for all the reactions investigated in this study. Figure 3.2 shows the photographs of the reaction mixtures (CdSe nanocrystal and Pd salt solution) taken several minutes after mixing the reactants under condition (A)-(C). The difference in the extent of reaction can be seen from the colors of the reaction mixtures, since the initial color of CdSe nanocrystal turns dark brown as the reaction proceeds. For the reaction CdSe $\rightarrow$ PdSe with 5nm CdSe nanocrystals, the reaction completed on the order of 10 minutes under condition (C). Under condition (A), the product often precipitated with only partial cation exchange during the same reaction time. Condition (B) resulted in the least extent of reaction among the three reaction conditions.

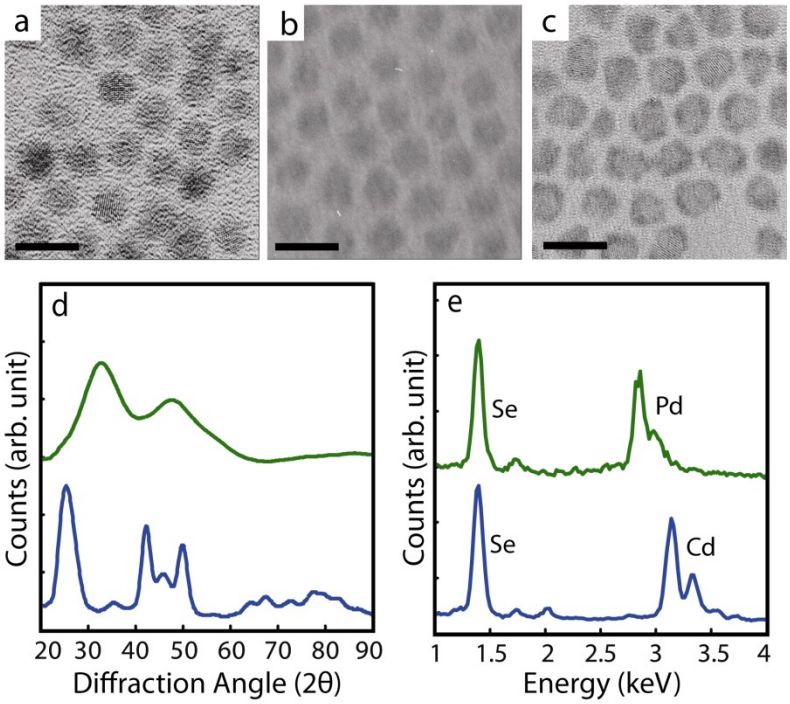

Figure 3.3. TEM images of (a) reactant CdSe nanocrystal, (b) fully cation-exchanged product PdSe, and (c) partially cation-exchanged PdSe nanocrystals from the reaction CdSe → PdSe. Scale bars are 10 nm. (d) XRD patterns and (e) EDX spectra of CdSe (blue) and PdSe (green) nanocrystals.

Figure 3.3(a) to (c) compares the TEM images of the reactant and products nanocrystals for the reaction CdSe → PdSe under conditions (A) and (C), where the partially and fully cation-exchanged nanocrystals were formed respectively. Completion of the cation exchange was confirmed by XRD and EDX analysis, Figure 3.3(d) to (e). In the case of full cation exchange reaction, exchange ratio between Cd and Pd cations was approximately 1:1 based on the EDX measurement. For partially exchanged nanocrystals, Figure 3.3(c), only the outer surface of the nanocrystal was exchanged, while maintaining 1:1 exchange ratio of the cations. In the EDX spectra, the small peaks around 1.75 and 2 keV are silicon and phosphorus respectively. The phosphorus is from the surfactants used in the cadmium chalcogenide nanoparticle synthesis and the silicon is from grease that is used on the ground glass joints in the experimental setup.

It is relatively easy to understand the differences in the efficiency of the cation exchange reaction under different solvent medium condition. Under condition (C), DDAB acts as the phase transfer catalyst selectively for Pd cations bringing CdSe nanocrystal and Pd cation into the same phase. Pd and Pt cations are known to form DDA-metal chloride complex via quaternary nitrogen, which gives solubility in nonpolar solvents.[72] Transfer of Pd and Pt cations from aqueous to organic phase occurred within seconds after shaking the reaction mixture, which was easily seen from the disappearance of the color of metal ions in the aqueous phase. On the other hand, the exchanged Cd cations were solvated preferentially in the aqueous phase, separated from the product nanocrystals in the organic phase,

since DDAB does not complex with Cd cations efficiently.[73] Such a condition should provide a strong thermodynamic driving force for the forward reaction, consistent with the most effective reaction observed under condition (C).

Under condition (A), the advantage of isolating Cd cations from the product nanocrystals and Pd or Pt cations via selective solvation does not exist. Methanol provides a favorable condition for solvating all ionic species present in the reaction mixture. The equilibrium of reaction will depend on the relative stability of cations solvated by the same medium in addition to the relative thermodynamic stability of the reactant and product nanocrystals. Under condition (B), nonpolar solvent medium disfavors the solvation of Cd cations, while Pd and Pt cations can exist stably in nonpolar medium with the help of DDAB. Inefficient reaction under condition (B) is probably due to the unfavorable solvation condition for Cd cations. However, adding a few drops of methanol or water into the reaction mixture of condition (B) immediately shifted the equilibrium to the forward direction by creating a reaction condition similar to (C). These observations clearly demonstrate the importance of cation solvation condition in determining the thermodynamic driving force and efficiency of the reaction. Considering that typical solvation energy of divalent cations in aqueous medium is about -400 kcal/mole,[74] strong dependence of the equilibrium on cation solvation condition is not unexpected.

Immediate shift of the equilibrium by a small change in the solvent environment discussed above also confirms relatively low activation barrier of the cation exchange reaction in nanocrystals. However, the reaction CdSe $\rightarrow$ PdSe

exhibited much slower kinetics compared to CdSe → Ag_2Se studied earlier suggesting higher activation barrier. In order to further examine the reversibility of the reaction, an attempt to induce the reverse reaction PdSe → CdSe was made. In the case of Ag_2Se, reverse reaction was completed within a minute when excess amount of Cd cations was added to the solution of Ag_2Se nanocrystals under ambient condition. When PdSe nanocrystals were put under the same reaction condition, the reverse reaction was not observed even with several hours of reaction time, confirming the higher activation barrier than the case of Ag_2Se. Cation exchange reactions of CdS and CdTe with Pd and Pt cations exhibited the same trend of solvent-dependent equilibrium as observed in reaction CdSe → PdSe. However, the reactions were generally faster in order of telluride to sulfide. Completion of reaction CdTe → PdTe occurred in several minutes, while CdS → PdS required ~1 hour of reaction time under condition (C).

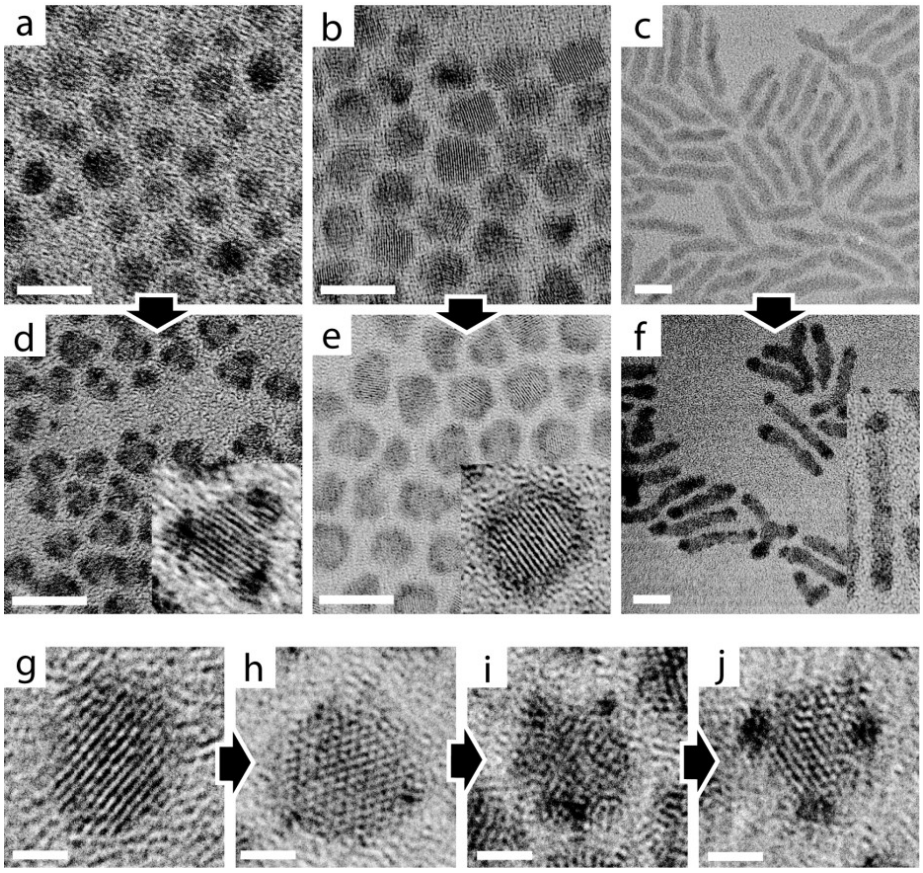

Figure 3.4. TEM images of (a-c) reactant, and (d-f) partially cation-exchanged product nanocrystals from the reactions CdE → PdE (E=S or Se). (a-c) are the images of CdS sphere, CdSe sphere and CdSe rod, respectively. (d-f) corresponds to the products from (a-c), respectively. Inserts in (d-f) are high resolution images of the product nanocrystals in each panel. Scale bars in (a-f) are 20 nm. (g-j) High resolution TEM images showing the progression of the cation exchange on zinc blend CdS nanocrystals with Pt cations. Scale bars in (g-j) are 2 nm.

3.2.2 Morphology of the partially cation-exchanged nanocrystals

In cation exchange reaction of the nanocrystals, the anisotropic morphology of the nanocrystals was often preserved after the reaction.[35, 52, 59] This indicates that the frame of the anion sub lattice was maintained with only minor adjustments of the ion positions, while cations were completely exchanged. In this case, the reaction can be viewed as the diffusion of cations through the anion sub lattice that has a limited flexibility. An interesting question that arises is where the exchange of cations initiates on the nanocrystal and how the reaction propagates. To address this question, intermediate structures with partial cation exchange were investigated. Partially cation-exchanged products were obtained by precipitating and washing the product nanocrystals before the completion of the reaction.

Figure 3.4 (a) to (f) compare the TEM images of the partially Pd-exchanged nanocrystals produced from CdS and CdSe spheres and CdSe rods. In the case of zinc blend CdS nanocrystals, Figure 3.4 (a) and (d), the regions of the reaction on the nanocrystals coincide with the apexes of the tetragonal pyramid. Exchange with Pt cations also resulted in the partially Pt-exchanged nanocrystals of the same morphology. Figure 3.4 (g) to (j) shows the progression of the exchange reaction in zinc blend CdS nanocrystals by Pt cations. Interestingly, the shape of the nanocrystals becomes more faceted as the reaction continues. On the other hand, partial cation exchange occurred homogenously on the outer surface of the sphere in the case of wurtzite CdSe nanocrystals, Figure 3.4 (b) and (e), in contrast to CdS nanocrystals. In wurtzite CdSe nanorods, Figure 3.4 (c) and (f), the reaction

occurred preferentially at both ends of the rod under condition (A), while the preference was weakened under condition (C). These observations clearly demonstrate that the initiation and progress of the cation exchange reaction depends on the lattice structure and morphology of the reactant nanocrystals.

Preferential reaction at the tip of CdSe nanorods is reminiscent of the formation of the semiconductor nanorods by solvothermal methods or reduction of gold at the tip of semiconductor nanorods.[9, 58] Anisotropic reaction to form nanorods has been explained in terms of different accessibility of reactant monomer to the different regions of the nanocrystals due to the selective passivation of particular faces of the lattice by the surfactant molecules.[9] An analogous argument may be made to explain preferential exchange reaction at a particular region of the nanocrystals observed in this study. In combination with the steric factor described above, generally higher reactivity at the regions with higher surface curvature and lower coordination number may also have played a role in determining the preferred site for the initiation of the reaction.[26] Formation of the partially Pd and Pt-exchanged zinc blend CdS nanocrystals, where the reaction occurred at four apexes of the tetragon, may be explained in this way.

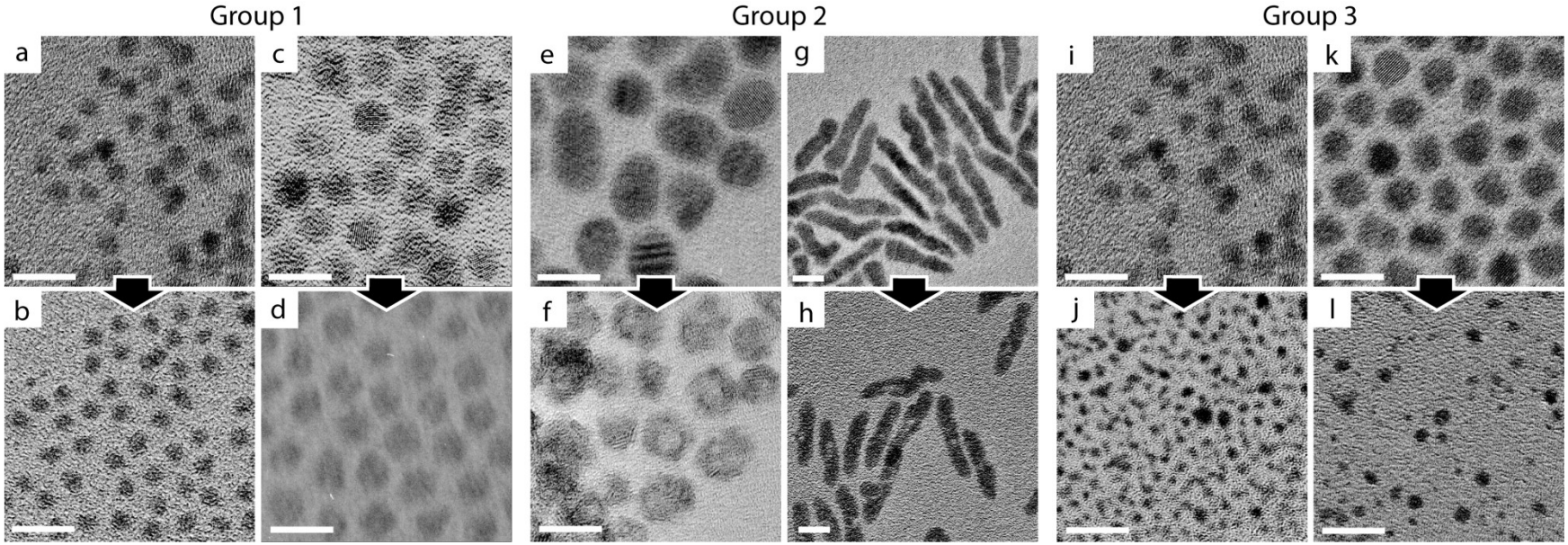

Figure 3.5. TEM images of the reactant CdE (E=S,Se,Te) and fully exchanged product nanocrystals. Reactant-product pair is indicated by an arrow connecting the two panels. (a-b) CdS-PdS, (c-d) CdSe-PdSe, (e-f) CdTe-PtTe, (g-h) CdSe-PdSe, (i-j) CdS-PtS, (k-l) CdSe-PtSe. Scale bars are 10nm.

3.2.3 Structure and morphology of the fully cation-exchanged nanocrystals

Figure 3.5 compares the morphologies of the initial reactant and fully cation-exchanged product nanocrystals from the reactions $CdE \rightarrow M_xE_y$, (E= S, Se, Te and M=Pd, Pt). The reactions are categorized into three groups according to the nature of the morphology change as will be discussed in detail below.

In order to characterize the lattice structure of the fully cation-exchanged nanocrystals, XRD patterns of the reaction products were obtained. Figure 3.6 compares the XRD patterns of the reactant (blue) and product (green) phases. However, the identification of the lattice structures of the product phase from XRD pattern alone was not straightforward due to the very broad diffraction peaks and the existence of multiple phases of Pd and Pt chalcogenides.

For Pd-exchanged nanocrystals, the exchange ratio between Pd and Cd cations obtained from EDX measurements was approximately 1:1, indicating the average oxidation state of +2 for Pd. Based on this result, the expected phases of the product nanocrystals are PdS, PdSe and PdTe, which adopts tetragonal, tetragonal and hexagonal structure respectively in bulk phase. Considering the very broad diffraction peaks, it is likely that the product is in the disordered state of the corresponding bulk phase. Similarity of the experimental XRD patterns of PdS and PdSe nanocrystals to the theoretical XRD patterns calculated using their bulk lattice parameters with the extra peak broadening introduced (Figure 3.7), further supports the above conclusion.[75, 76]

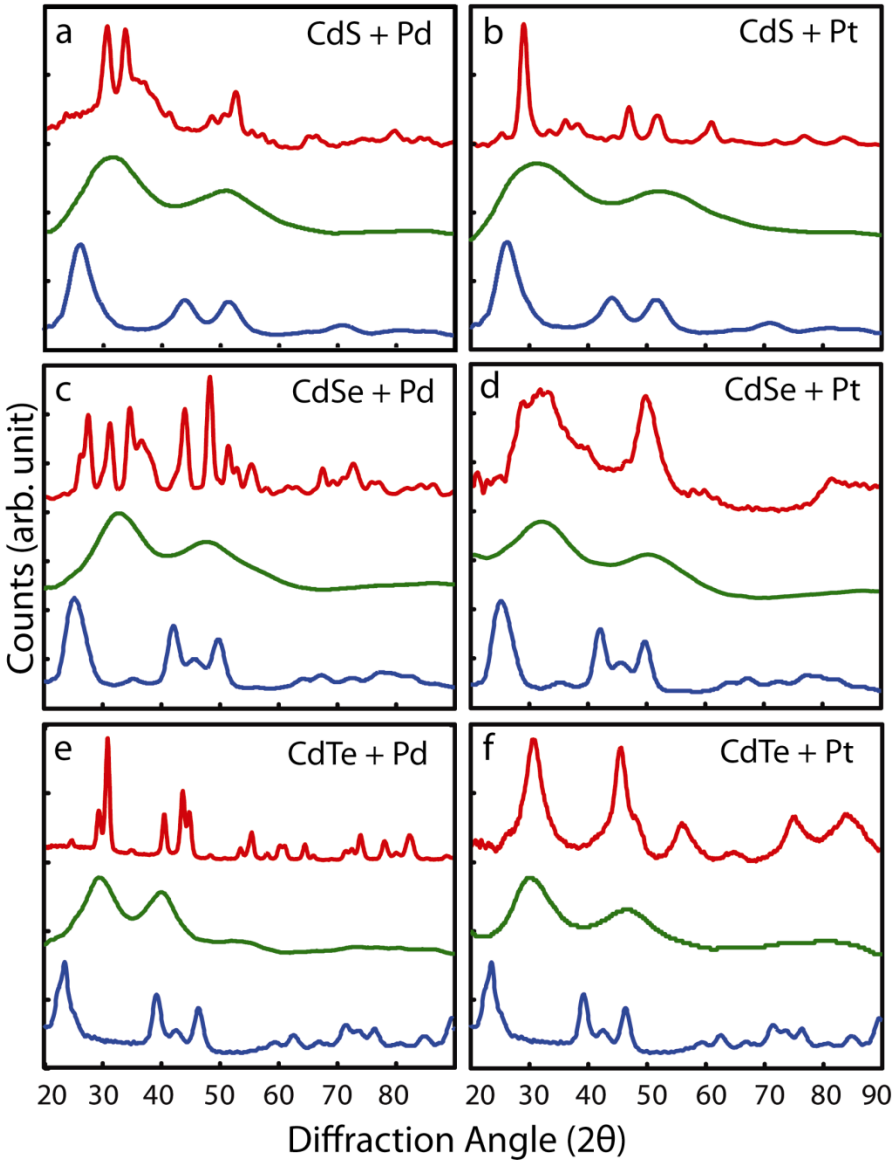

Figure 3.6. XRD patterns of reactant (blue), product (green) and thermally annealed product (red) nanocrystals from the cation exchange reaction CdE → M_xE_y, (E= S, Se, Te and M=Pd, Pt). Reactant nanocrystals and exchanging metal ions are indicated in each panel.

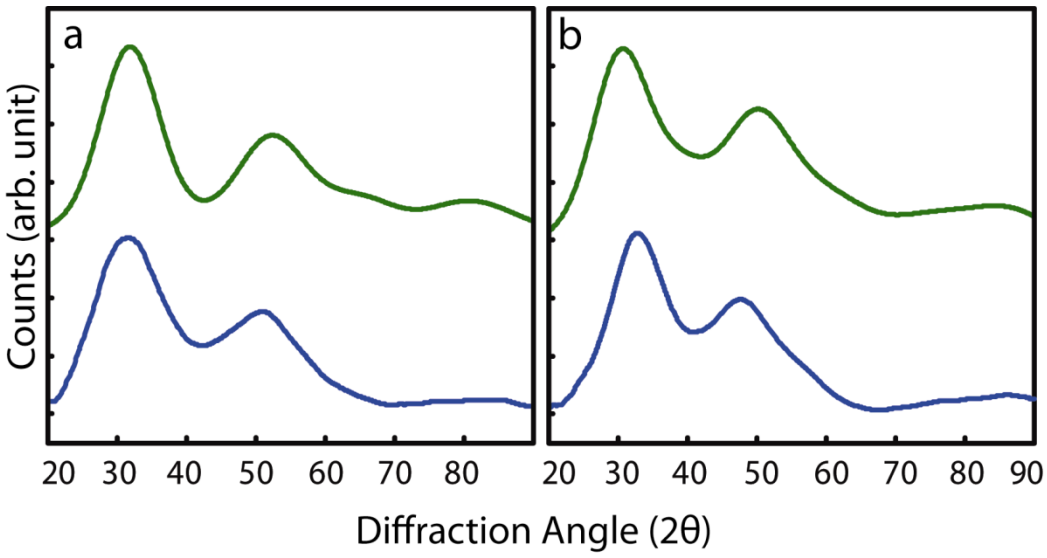

Figure 3.7. Experimental (blue) and simulated (green) XRD patterns of the fully cation-exchanged (a) PdS and (b) PdSe nanocrystals.

The theoretical peak broadening for the full width at half max calculations was done with PowderCell using FWHM = *f*(U,V,W). The crystal lattice constants were not changed. For the broadening for PdS, U was 20.00, V was 200.00 and W was 50.00. For the broadening for PdSe, U was 0.00, V was 100.00 and W was 50.00. While only the simulated broadened XRD of PdS and PdSe are showing in Figure 3.7, the other systems (PdTe, PtS, PtSe and PtTe) were also analyzed. It was found that all amorphous XRD data could be fit to simulated XRD using peak broadening.

In the case of Pt-exchanged nanocrystals, the cation exchange ratio and the oxidation state of Pt cations in the product phase measured from x-ray photoelectron spectroscopy (XPS) was more complex, Figure 3.8. For sulfide, the oxidation state of Pt cations was +2, consistent with the observed Pt:S ratio of 1:1 in the product nanocrystals. In telluride, Pt cations exhibited mixed oxidation states of +2 and +4, indicating more heterogeneous nature of the composition and structure.[77, 78] The XPS of PdSe nanoparticles is shown in Figure 3.9. Literature value of PdSe could not be found, but the experimental values fall between that of PdS and PdTe.[79, 80]

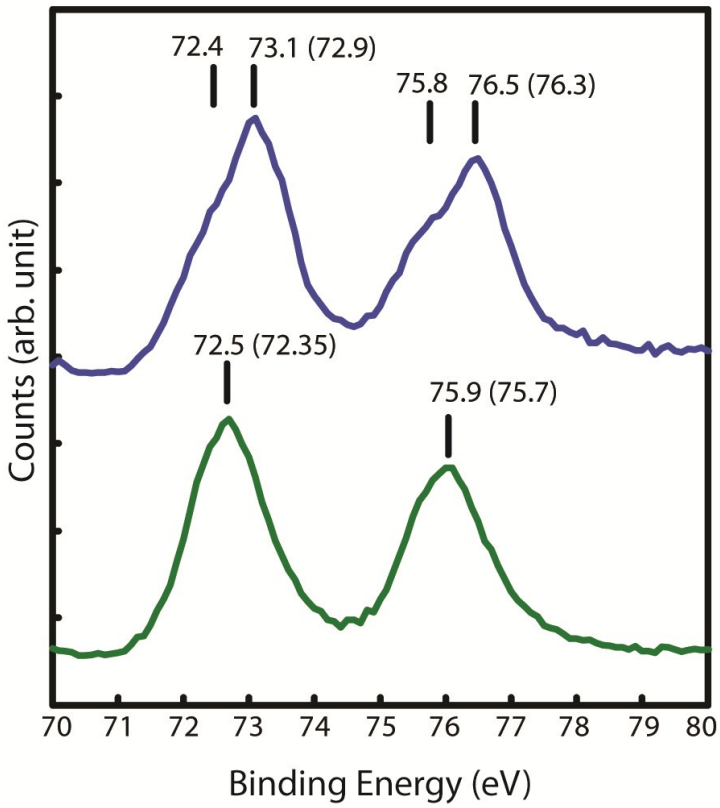

Figure 3.8. XPS spectra of (blue) PtTe and (green) PtS. The values in parentheses are taken from reported values in the literature.[77, 78]

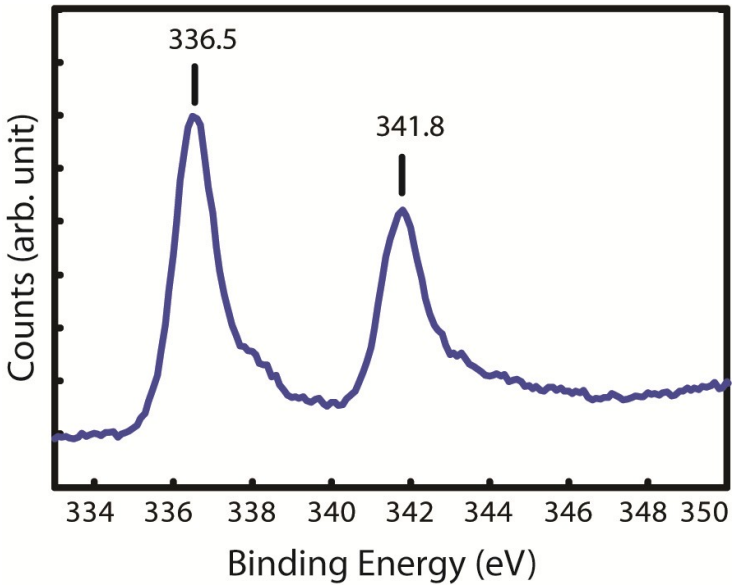

Figure 3.9. XPS spectrum of PdSe. For PdSe, literature values were not available; however, the experimental values are in between binding energies of Pd^{2+} for PdS and PdTe.[79, 80]

Table 3.2. Structure, lattice parameter and fractional volume change of reaction ($\Delta V/V$) for the reactant and possible product phases.

Material	**Structure**	**Lattice parameter**	**$\Delta V/V$**
CdS	Zinc Blende	a=5.82	Reactant
PdS	Tetragonal	a=6.43, c=6.61	-0.30
PtS	Tetragonal	a=3.47, c=6.10	-0.25
PtS_2	Rhombohedral	a=3.54, c=5.04	-0.44
CdSe	Wurtzite	a=4.30, c=7.01	Reactant
PdSe	Tetragonal	a=6.73, c=6.91	-0.30
$Pd_{17}Se_{15}$	Cubic	a=10.61	-0.29
$PtSe_2$	Rhombohedral	a=3.73, c=5.08	-0.45
Pt_5Se_4	Monoclinic	a=6.58, b=4.61, c=11.12	-0.27
CdTe	Wurtzite	a=4.57, c=7.44	Reactant
PdTe	Hexagonal	a=4.13, c=5.66	-0.38
PtTe	Monoclinic	a=6.87, b=3.96, c=7.04	-0.33
Pt_2Te_3	Monoclinic	a=6.93, b=4.00, c=17.12	-0.42
$PtTe_2$	Hexagonal	a=4.03, c=5.22	-0.46

If all the cation exchange reactions considered here produce stoichiometric products with bulk equilibrium structures, $\Delta V/V$ of reaction should range from -0.25 to -0.46 as shown in Table 3.2. In comparison, $\Delta V/V$ for CdSe $\rightarrow$ Ag_2Se studied earlier is only 0.06 with very little (<1%) changes in the lattice parameters.[35, 38] In principle, a decrease in volume and/or a change of shape of the product nanocrystals should be seen based on the theoretical values of $\Delta V/V$. However, TEM images in Figure 3.5 shows varying degree of morphology changes depending on the reaction and the size of the nanocrystals.

In Group 1, the product phase retains the original morphology. This is observed in the reaction of small CdS and CdSe nanocrystals with Pd ions. $\Delta V/V$ for these reactions is approximately -0.3. In the case of the reaction CdSe $\rightarrow$ PdSe, Figure 3.5(c) to (d), contraction of the plane perpendicular to the c-axis by about 30% is the major change of the structure.[69] However, contraction of the volume corresponding to such structural change is not apparent in the TEM images. It is possible that the product phase is kinetically frozen in a disordered and metastable state, where the lattice stress in sustained without conforming to the equilibrium lattice structure.

In Group 2, a void is formed inside the nanocrystals. This is observed in PdSe, Figure 3.5 (g) to (h), and PtTe, Figure 3.5(e) to (f), especially for larger nanocrystals. The void formation may be explained in terms of the release of the stress in the lattice accumulated in the product phase during the reaction.[81] The stress that was sustainable during the early phase of the reaction may have reached

a critical point, which triggered the formation of the void from interior releasing the stress in the lattice. Although the formation of the void is seemingly analogous to the Kirkendall effect observed in earlier studies of Co_xS_y nanocrystals,[49] the origin of the void formation is different. In the case of the Kirkendall effect, void formation is driven by the disparity of the diffusion coefficients of the two chemical species propagating in the opposite direction. However, in the case of the cation exchange reaction, it is the static anion sub lattice that determines the morphology of the nanocrystals after the reaction.[37]

In Group 3, fragmentation of the nanocrystals to smaller pieces occurred. This was observed in the reactions of CdS and CdSe nanocrystals with Pt cations, Figure 3.5(i) to (l). Fragmentation may have resulted from continuous break-off of the ion-exchanged parts from the main body of the reacting nanocrystal due to the excessive lattice mismatch at the hetero interface. The resulting cation exchanged product nanocrystals were very heterogeneous in size and much smaller than the starting cadmium chalcogenide nanoparticles.

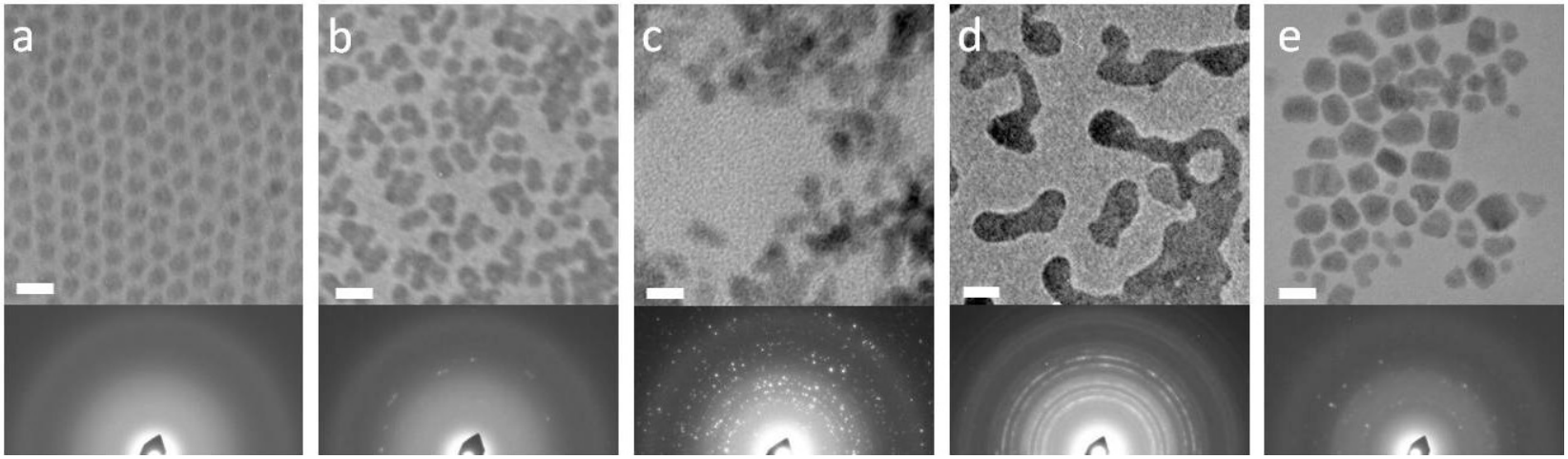

Figure 3.10. TEM images of in-situ PdSe nanocrystals under different in-situ heating conditions. (a) unheated, (b) 150 °C for 20 minutes, (c) 200 °C for 20 minutes, (d) 600 °C for 10 minutes. (e) TEM image of ex-situ heated PdSe in ODE at 200 °C for 20 minutes. Inserts are the electron diffraction patterns for each sample. Each scale bar is 10 nm.

3.2.4 Structure of the thermally annealed product nanocrystals

As discussed above, the product nanocrystals from cation exchange reaction may have a significant lattice stress and disorder especially when the product nanocrystals did not conform to the expected change of volume. In that case, the product nanocrystals may transform to the thermodynamically more stable and ordered phase via thermal annealing of the lattice. In order to see if the metastable and disordered structure of the reaction product can relax to more equilibrated structure, an in-situ TEM measurement of the thermally annealed product nanocrystals was made. Thermal annealing was done by heating the nanocrystal sample deposited on thin Si_3N_4 substrate in-situ on the temperature-controlled sample holder of TEM. The sample was heated at several different temperatures. The TEM image and electron diffraction patterns of the thermally annealed sample were taken after cooling the sample stage to the ambient temperature.

Figure 3.10 shows the TEM images and electron diffraction patterns of the PdSe nanocrystals before and after thermal annealing. After heating at 150 °C for 20 minutes, Figure 3.10(b), the nanocrystals exhibit a noticeable reduction in size compared to the unannealed PdSe nanocrystals, Figure 3.10(a). This is consistent with our assumption that thermal annealing will transform to more equilibrated structure of the product phase with $\Delta V/V$ of -0.3. However, the structure of the lattice still seems disordered based on the lack of well-defined diffraction patterns.

After further heating at 200 °C for 20 minutes, the nanocrystals began to form a crystalline phase with the increasing extent of agglomeration, Figure

3.10(c). The electron diffraction pattern in Figure 3.10(c) corresponds to $Pd_{17}Se_{15}$. With continued heating at a higher temperature, the nanocrystals melted completely. The diffraction pattern obtained after cooling down to the ambient temperature clearly shows the diffraction rings corresponding to $Pd_{17}Se_{15}$, Figure 3.10(d). However, it is not entirely clear if the transformation to $Pd_{17}Se_{15}$ is purely structural annealing or chemical disproportionation. In bulk phase, PdSe can disproportionate into $Pd_{17}Se_{15}$ and $PdSe_2$ above ~600 °C.[82] What is observed in Figure 3.10(c) to (d) may be the combined result of structural annealing and disproportionation. Ex-situ thermal annealing of PdSe nanocrystals in octadecene at 200 °C for 30 minutes also yielded $Pd_{17}Se_{15}$ nanocrystals. However, the annealed nanocrystals were much larger than the original PdSe nanocrystals due to the agglomeration. Other reaction products also exhibited agglomeration and crystallization to more equilibrated structure upon ex-situ heating. XRD patterns of the ex-situ heated samples are shown in Figure 3.6 (red curve in each panel). Crystalline tetragonal PdS and PtS were formed from thermal annealing of the disordered product nanocrystals. Heating of PdSe resulted in $Pd_{17}Se_{15}$ as described above. Thermal annealing of the disordered PdTe resulted in mixed phases of PdTe and $PdTe_2$.

3.3 Conclusions

We have shown that equilibrium of the cation exchange reaction in nanocrystals can be significantly changed by modifying the cation solvation condition of the solvent medium. In particular, the equilibrium of the cation exchange reaction could be shifted toward the formation of the product via selective solvation of cations in a particular solvent phase. The effect of large volume change of reaction on the morphology of the product phase has also been studied. This is a particularly important issue when the reactant nanocrystal acts as a morphological template. Depending on the stress developed in the lattice during the reaction due to the difference of the lattice structure between the reactant and product, the product nanocrystals underwent varying degree of morphological changes, such as void formation and fragmentation. The knowledge on the effect of ion solvation and ΔV of reaction on the equilibrium and product morphology obtained from this study provides a new strategy and useful guides to the application of cation exchange reactions for the synthesis of a broader range of inorganic nanocrystals.

CHAPTER IV

TERNARY I-III-VI_2 CHALCOGENIDE NANOPARTICLES

4.1 Introduction

Ternary I-III-VI_2 chalcopyrites and their solid solutions have received much attention in the applications in photovoltaic and thermoelectric devices.[43-45] For example, $CuInSe_2$ has a high absorption coefficient, suitable band gap (around 1 eV) and stability in the sun's radiation which lends well for its application in solar cell devices.[30] In addition, these materials are more environmentally friendly, seeing as they do not contain toxic metals such as Cd (CdSe and CdTe have been studied and proposed for solar cell applications as well).

$CuInSe_2$ has two different structures, sphalerite and chalcopyrite. Chalcopyrite is a crystal structure, similar to zinc blende, but with two different cations with one anion. The anion is surrounded by two of each type of cation, and each cation is surrounded by four anions. Due to the unequal sizes of the two cations, there is tetrahedral distortion in contrast to the zinc blende structure. Figure 4.1 illustrates the $CuInSe_2$ chalcopyrite phase with yellow being Se, red being Cu and blue being In. The sphalerite phase is similar to the chalcopyrite in that they have the same anion sublattice, but the arrangement of the cations are different in that they are randomly distributed. The chalcopyrite is the thermodynamically stable phase and the phase most desired for $CuInSe_2$ applications in devices. When synthesizing nanomaterials of $CuInSe_2$, it has been found that the order of addition of the Se

precursor can actually lead to the different phases of $CuInSe_2$, which illustrates how important it is to control the synthetic parameters to obtain the desired materials.[83] For the remainder of this thesis, it will be implied that when talking about $CuInSe_2$ it is the chalcopyrite phase unless otherwise indicated.

Temperature, elemental precursors, order of addition of the precursors and reaction time are just a few of the experimental conditions that need to be controlled to make the desired nanoparticle shape, size and composition. For $CuInSe_2$, balancing three different elemental precursors with different reactivity is one of the many reasons why the synthetic methods of $CuInSe_2$ (or any ternary nanomaterials) are difficult. The properties of I-III-VI_2 chalcopyrites depend on the composition of the material; therefore, syntheses that make nanoparticles with reliable composition is important.[84, 85] In addition, the morphology of the nanoparticles is important, and there has been success in making $CuInSe_2$ nanomaterials of different morphology. For example, tetrahedron $CuInSe_2$ nanoparticles were made using oleylamine as the solvent and surfactant with CuCl, $InCl_3$ and selenourea as the elemental sources.[86] Larger structures of hexagonal microplates were made in a combination of oleylamine and oleic acid with elemental selenium and the acetylacetonate salts of copper and indium.[87] A nanoring morphology has even been made which used oleylamine, trioctylphosphine, selenium, copper (I) chloride and indium trichloride.[83]

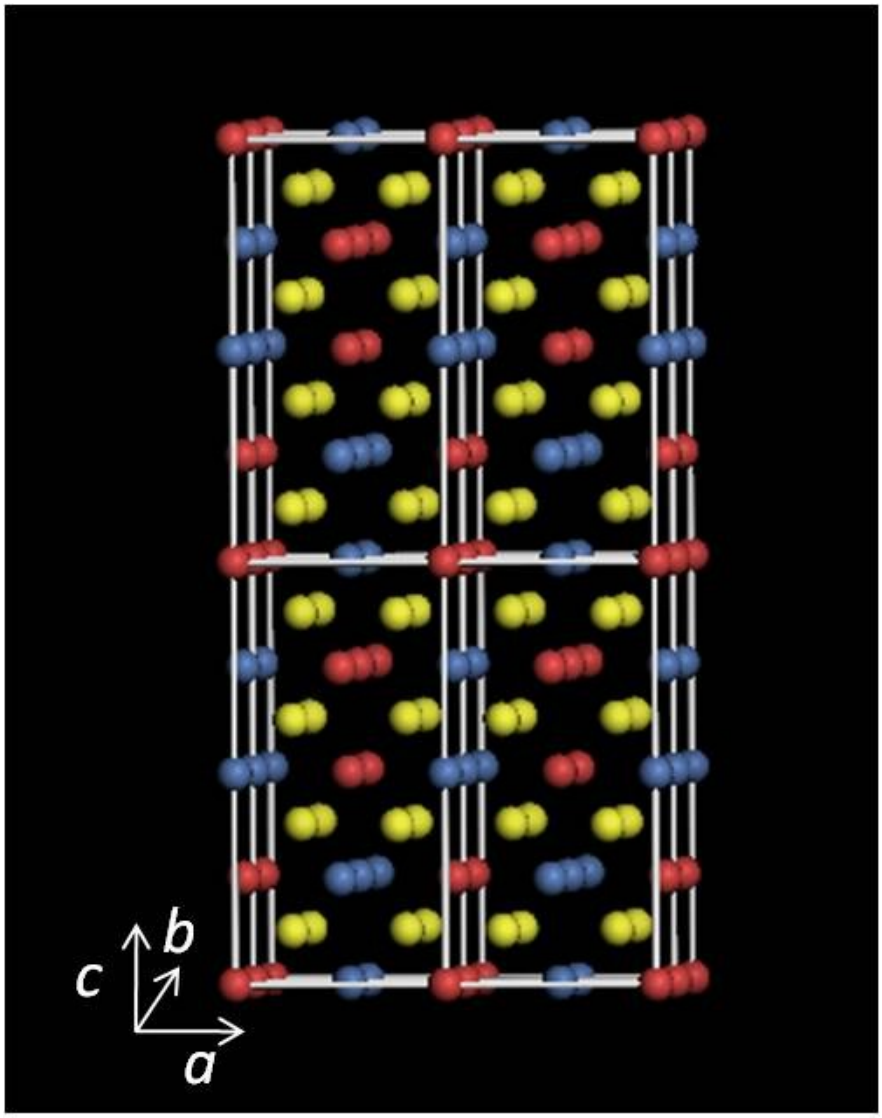

Figure 4.1. Crystal structure of chalcopyrite $CuInSe_2$. Yellow, blue and red represent selenium, indium and copper, respectively.

From the previous examples, it can be seen that synthetic methods with very similar compounds yield very different morphologies. In general, the synthetic methods that have been published focus more on the study of the material properties of the synthesized substance, but no real progress has been made in understanding the major synthetic variables of the Cu-In-Se system.

4.2 Methods to make anisotropic shaped nanoparticles

Recently, nanostructured chalcopyrites, particularly nanowires among other structures, have attracted significant interest due to the advantages that 1-dimensional nanostructures can offer in their device applications.[83, 88, 89] Smooth, single crystal, one-dimensional structures offer natural charge transport conduits while rough one-dimensional structures may scatter phonons effectively and be useful in thermoelectric materials. Due to the potential applications, understanding how to make anisotropic ternary chalcogenide nanomaterials is of importance.

To understand the growth of anisotropic nanoparticles, an understanding of the growth of isotropic nanoparticles is helpful. The growth of nanoparticles is typically split into two stages, nucleation and growth. Nucleation occurs after the reaction solution becomes supersatured with the monomer precursor. Growth takes place after nucleation and incorporates the monomers left in the reaction solution. If growth is left unchecked, then a corseting of the size distribution of the nanoparticle will result. Researchers often try to separate these events, nucleation and growth, to obtain better control over the resulting size and shape of the

nanoparticles. If the synthesis is kinetically controlled, then the rate at which the different crystal faces grow dictates the shape of the nanocrystal. If the reaction is thermodynamically controlled, then the resulting shape is due to a minimization of the surface energy.

For the synthesis of anisotropic semiconducting nanoparticles, several growth mechanisms have been proposed.[4, 6, 90] The simplest model uses thermodynamics to explain the shape control over crystals. The final shape of the crystal will be determined by minimization the total free energy of the system. This method has been useful in explaining some shape control in nanoparticles; however, it cannot explain shape evolution in a single surfactant system.[4]

The selective-adsorption model explains how a mixed surfactant system leads to anisotropic growth. Having two or more surfactants that selectively adsorb to different crystal faces changes the surface free energy, allowing different crystal faces to have unequal reactivity.[91] The selective-adsorption model though cannot explain anisotropic growth in single surfactant systems. For anisotropic growth in a single surfactant system, typically multiple injections are used to maintain monomer concentration. By maintaining a sufficiently high monomer concentration, the relative differences in the different crystal faces' growth rate can be maintained, leading to anisotropic growth.[91]

Another type of mechanism that leads to anisotropic growth is the oriented attachment model. Oriented attachment lowers the surface tension through attachment of two smaller particles at a similar crystal face. This process can be

controlled through the controlled removal of surfactants on the surface, which was shown in CdTe "pearl necklaces".[92] Oriented attachment illustrates the need to understand how nanoparticles interact with each other, specifically the looking at the intermolecular forces between them, such as dipole-dipole interactions.[4]

Solvents and surfactants can also act as molecular templates, which act as a scaffold for nanomaterials to go on. This scaffold can be compared to a template, and has been proposed in nanoparticle synthesis that uses ethylenediamine as solvent and surfactant. While this model has been suggested, more experimental proof is still needed.

Micelles have been used as a solution based method used to make a variety of composition and shaped nanoparticles. The micelle method uses a surfactant molecule that has both hydrophobic and hydrophilic interactions to spontaneously form small surfactant aggregates of micelles that are typically spherical. If more than one surfactant is used, other shapes can be made such as nanorods. The mixed surfactant micelle system is similar to the one previously discussed of selective adsorption, but due to the weaker binding of the micelle surfactants, it is probably not the case.[4]

The final solution phase mechanism that will be discussed uses catalytic nanoparticles to direct the anisotropic growth in nanomaterials. Solution-liquid-solid (SLS), analogous to vapor-liquid-solid (VLS) growth mechanism, has been shown to be very useful in making uniform nanowires.[93] The catalytic nanoparticle in solution directs anisotropic growth, but only at the interface between the

nanoparticle and the growing semiconductor is growth seen. The diameter of the wires is dependent on the size of the catalytic nanoparticle.[93] The nanoparticle catalysts used must be molten under the reaction conditions to allow one of more of the elemental precursors to be somewhat soluble to allow for supersaturation and subsequent one-dimensional growth. The catalytic nanoparticles can either be formed as a side product to the desired crystal phase or can be systematically added into the reaction mixture. It was found that systematically adding known concentrations and sizes of nanoparticles allowed for more controlled nanowire synthesis.

While not a solution based method, template based methods such as AAO tubes have shown success in making anisotropic nanoparticles, specifically nanowires. The AAO tubes can vary in diameter from 10 to 2000 nm and the composition can be varied by changing precursor mixtures. The nanowires are electrochemically formed and, by changing the reaction conditions, can make wires that range from a single material to more complex structures such as stripped heterostructure with multiple materials.[94, 95]

4.3 Overview of $CuInSe_2$ nanowire synthesis

Nanowires of various binary and ternary chalcogenide materials have been prepared in a number of different ways.[96-98] Among the methods that do not rely on templates (e.g. anodic aluminum oxide tubes), the following two methods are the most commonly used. One method is using metal nanoparticles as the catalyst

directing 1-dimensional anisotropic growth, in either vapor-liquid-solid (VLS) or solid-liquid-solid (SLS) growth. The other option is solution phase synthesis involving heating of precursors in a mixture of liquid solvent with surface-passivating surfactants. Solution-phase synthesis of 1-dimensional structures that do not use a metal nanocrystal catalyst or template rely on the anisotropic crystal growth assisted by the anisotropic adsorption of surfactant molecules on different facets during growth.[9, 99] Both methods are relatively well established for the growth of various binary semiconductor materials with some success applied to ternary semiconductor materials.[73, 100] However, it is generally more challenging to synthesize ternary nanowires that are chemically and structurally homogeneous due to the added complexity of the phase diagram and reaction kinetics of the multi-component system.

In the case of $CuInSe_2$, which is considered one of the most promising materials in photovoltaic applications, preparation of nanowires from VLS and SLS growth has been recently demonstrated by a number of groups.[73, 100, 101] Methods based on templating have also been used to form 1-dimensional structures.[89, 102, 103] Solution-phase synthesis of $CuInSe_2$ nanowires without a metal nanocrystal catalyst or template has been less successful most likely due to the insufficient structural anisotropy of the double zinc blende structure and weak anisotropic surfactant passivation. So far, $CuInSe_2$ nanocrystals of spherical and several other shapes, such as tetrahedron, hexagonal plate or nanowiskers, have been made.[86, 104-107]

In this report, we describe a solution phase synthesis method that produces multi-micron length nanowires of $CuInSe_2$ without using a metal nanocrystal catalyst. We show that the growth of $CuInSe_2$ nanowires can be achieved by using only a moderately binding surfactant, which may enhance the relatively weak intrinsic anisotropy of the crystal growth. Since the shape of the nanocrystals in solution phase synthesis depends on the surface energies of different facets that decreases when passivated by the surfactant, the affinity of the surfactant molecules is important in determining the nanocrystal shape.[6] When the surfactant is strongly adsorbing, the crystal facets with small intrinsic anisotropy may be passivated without sufficient selectivity required for anisotropic growth. However, surfactants with more moderate binding affinity will be less indiscriminate passivating different facets potentially resulting in the stronger tendency for anisotropic growth than with more strongly binding surfactants.

In this work, DOPO was identified as the key surfactant that leads to the continuous growth of nanowires from anisotropic passivation of different facets.[108] The synthesized nanowires often exhibited a saw-tooth pattern on the surface that resembles a stack of truncated tetrahedra. The coherency of the lattice was maintained better along the axial direction, while twinning around the growth axis was observed. The highly modulated surface morphology in nanowires could be potentially useful for nanoscale thermoelectric applications.[109-112]

CHAPTER V

SOLUTION-PHASE SYNTHESIS OF VARIOUS MORPHOLOGIES OF $CuInSe_2$ NANOPARTICLES*

5.1 Experimental section

5.1.1 Materials

The following chemicals were purchased from Aldrich and used without further purification: Trioctylphosphine Oxide (TOPO 99%), copper (I) chloride (CuCl ≥99%), indium trichloride tetrahydrate ($InCl_3 \cdot 4H_20$, 97%), indium trichloride ($InCl_3$), selenium powder, oleylamine (technical grade, 70%), octylmagnesium bromide in diethyl ether (2M), dibutylphosphite (96%), potassium carbonate (K_2CO_3), octadecene (technical grade, 90%) and copper(II) acetylacetonate ($Cu(acac)_2$). The following chemicals were purchased from Strem and used without purification: TOPO (99%), trioctylphosphine (TOP, 97 %)

5.1.2 Synthesis of $CuInSe_2$ nanowires

$CuInSe_2$ nanowires were made in solution phase using 10^{-3} mole (0.10 g) of CuCl and 10^{-3} mole (0.29 g) of $InCl_3 \cdot 4H_20$ which were added into a mixture of 1.2 g of TOPO, 0.8 g of dioctylphosphine oxide (DOPO) and 3 ml of TOP in a flask. The

---

* Reprinted in part with permission from *J. Mater. Chem.*. Wark, S. E.; Hsia, C. H.; Luo, Z.; Son, D. H., Surfactant effect on the formation of $CuInSe_2$ nanowires in solution phase synthesis. *J. Mater. Chem.*. **2011**, DOI:10.1039/C1JM10401B

experimental set up is illustrated in figure 3.1. The flask was degassed under vacuum at 100 °C for 1 hour. After refilling the flask with N_2, the reaction mixture was heated to 260°C. To initiate the reaction, 2 ml of 1M solution of Se in TOP (TOP:Se) was injected into the flask. After 2-6 hours of reaction, the reaction mixture was cooled down to room temperature and 20 ml of toluene was added. The collected nanowires were rinsed in ethanol and precipitated repeatedly to remove the remaining organic surfactants and other impurities.

Variations of this procedure using different solvent and surfactant molecules were also used to investigate the effect of varying surfactant binding affinity on the morphology of $CuInSe_2$ nanocrystals. The amount of TOPO plus DOPO was held at a constant 2.0 g. The ratio of the two was varied to study the resulting morphology of the nanoparticles. In addition, ODE was substituted for TOPO, to understand the role of TOPO in the synthesis. 1.2 ml of ODE was substituted for the 1.2 g of TOPO in the nanowire synthesis.

As a side note, the reaction solution was found to be reactive with the thermocouple used, prohibiting the formation of $CuInSe_2$. To combat this problem, a glass sleeve was used over the thermocouple. A slight amount of ODE was added to the glass sleeve to assure that the thermocouple would read the correct temperature of the solution in the round bottom flask. ODE was chosen because it is a high boiling point solvent that is nonreactive.

5.1.3 Synthesis of $CuInSe_2$ nanospheres

Small $CuInSe_2$ nanoparticles were synthesized following a previously reported method.[104] $2 \cdot 10^{-4}$ mole (0.053 g) of $Cu(acac)_2$ (99.99 %, Aldrich) and $2 \cdot 10^{-4}$ mole (0.044 g) of $InCl_3$ (98 %, Aldrich) were added to 5ml of oleylamine (70 %, Aldrich) in a flask and degassed at 100 °C for 1 hour then backfilled with N_2 and allowed to cool. Se dissolved oleylamine (OA:Se) was prepared by heating 0.04 g ($5 \cdot 10^{-4}$ mole) of Se powder in 8ml of oleylamine at 250 °C for 1 hour. The precursor solution of Cu and In was then quickly injected into the hot OA:Se solution. After 30 minutes of reaction, the flask was cooled down to room temperature. Typically spherical particles of >10 nm in diameter were formed in this way. To clean the sample, 10 ml of toluene was added to the reaction solution and then methanol was added until the solution became turbid. The solution was then centrifuged and the supernatant was discarded. The precipitate was then redissolved in toluene. Two more washings by methanol precipitation were then performed.

Larger spherical nanocrystals (50-250 nm in diameter) were synthesized using the procedures similar to that of the nanowires. While the same Cu, In and Se precursors were used, the reaction occurred in the mixture of TOPO (2 g), TOP (1 ml) and oleylamine (2 ml). The size of the nanocrystals was varied by varying the reaction time. Growth could be seen in less than one minute and at 2 minutes the $CuInSe_2$ spheres were already 80 nm in diameter. If the small or large spherical nanocrystals were not cleaned after synthesis, etching would occur due to

oleylamine. The synthetic conditions of the different types of $CuInSe_2$ nanoparticles are summarized in Table 5.1.

5.1.4 Structural characterization of the nanocrystals

The crystal structures of the synthesized nanocrystals were examined using XRD and electron diffraction. Powder XRD patterns were obtained on a Bruker-AXS GADDS diffractometer equipped with copper X-ray source and multi-wire proportional counter as the detector. Electron diffraction patterns of the nanocrystals were obtained on a JEOL 2010 TEM at an acceleration voltage of 200 kV. The same instrument, equipped with Oxford Instruments INCA EDX system, was used to obtain both TEM images and elemental composition of the nanocrystal samples. The 3-dimensional tomograms of the nanowires were obtained from a series of zero-loss energy filtered TEM images acquired from FEI Tecnai G^2 F20 FE-TEM (200 kV) equipped with a tilting sample holder with ±60° angle range. The TEM images taken at 1° tilt angle increment were processed with FEI Xplore3D software employing the back-projection method to reconstruct the 3-dimensional tomogram of the nanowires. The EDX analyses were done using FEI Tecnai F20 ST TEM, with an EDAX EDX detector. The EDX drift-corrected line scan was performed in the STEM mode using a beam spot size of 1 nm. Any specimen drifts during the scanning were corrected by choosing a reference area nearby. Nickel TEM grids were used instead of Cu grids for the EDX measurements.

Table 5.1. Reaction conditions for $CuInSe_2$ nanocrystals shown in the figure on page 69.

	(a) small spheres	**(b) large spheres**	**(c) nanowires**	**(d) aggregates**
Solvent	Oleylamine, 5 ml	TOPO, 2 g Oleylamine, 2 ml TOP, 1 ml	TOPO, 2 g TOP, 3 ml	TOPO, 2 g TOP, 3 ml
Cu, In source	$Cu(acac)_2$, $2 \cdot 10^{-4}$ mole $InCl_3$, $2 \cdot 10^{-4}$ mole	CuCl, 10^{-3} mole $InCl_3 \cdot 4H_2O$, 10^{-3} mole	CuCl, 10^{-3} mole $InCl_3 \cdot 4H_2O$, 10^{-3} mole	CuCl, 10^{-3} mole $InCl_3 \cdot 4H_2O$, 10^{-3} mole
Se source	OA:Se, $5 \cdot 10^{-4}$ mole	TOP:Se, $2 \cdot 10^{-3}$ mole	TOP:Se, $2 \cdot 10^{-3}$ mole	TOP:Se, $2 \cdot 10^{-3}$ mole
Total volume	13 ml	7 ml	7 ml	7 ml
Reaction Time	30 minutes	30 minutes	4-6 hours	4-6 hours

5.1.5 Synthesis and characterization of dioctylphosphine oxide (DOPO)

DOPO, which is a key component for the synthesis of $CuInSe_2$ nanowires, was synthesized by employing a previously reported method.[113] The reaction scheme can be seen in Figure 5.1. 100 ml of 2 M octylmagnesium bromide in diethyl ether was added to a 250 ml flask under oxygen-free condition. While keeping the temperature of the flask in the range of 10-15 °C using an ice bath, 13.75 g of dibutylphosphite was added drop wise at a rate of 0.12 ml/minute. After all the dibutylphosphite was added, the temperature was raised to 35 °C to reflux for 30 minutes. Subsequently, the mixture was cooled down to 5-10 °C for the addition of 75 ml of 25 % aqueous H_2SO_4 solution over a 1 hour period. The ether layer containing DOPO was separated from the mixture and rinsed with 25 ml of 18.2 MΩ·cm deionized water three times. It was further rinsed with 25 ml of 15 % aqueous solution of K_2CO_3 three times and 25 ml of deionized water three times. Powder form of DOPO was obtained by evaporating ether at 65^{o}C. The dried DOPO was purified by recrystallization in n-hexane. The purity of the recrystallized DOPO was >97%. The identity and purity of DOPO were determined by electrospray ionization (ESI) mass spectrometry from the characteristic charge/mass ratio of 275 ($[DOPO+H]^+$), 297 ($[DOPO+Na]^+$) and 313 ($[DOPO+K]^+$) in the mass spectrum.

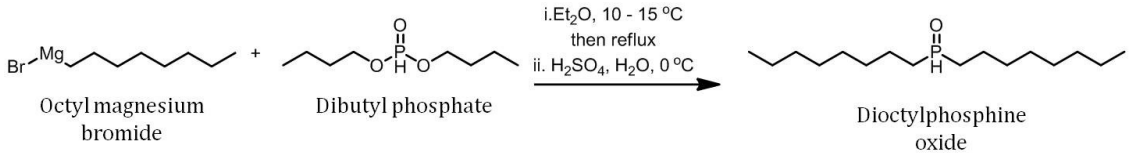

Figure 5.1. Reaction scheme illustrating the reaction of octyl magnesium bromice with dibutyl phosphate to make dioctylphosphine oxide.

5.2 Results and discussion

5.2.1 Effect of surfactant on the morphology of $CuInSe_2$ nanocrystals

Selective surface passivation of surfactant molecules during the nanocrystal growth is one of the key controls in solution phase synthesis of anisotropic nanocrystals, such as nanowires. If the binding affinity of the surfactant on different crystal facets is sufficiently different, unequal growth rates in different directions can result in anisotropic morphologies. This strategy has been successful in materials such as hexagonal wurtzite semiconductors, where the nanorods and nanowires were grown along the *c*-axis via preferential passivation of facets perpendicular to the growth axis.[9, 99, 113] On the other hand, 1-dimensional growth in zinc blende structures of these materials with cubic symmetry is more difficult due to the higher symmetry of the crystal structure.[114]

In the case of chalcopyrite $CuInSe_2$, the crystal structure is similar to zinc blende but with two different types of cations (Cu^+ and In^{3+}) distributed in the cation sites. Possibly due to the insufficient anisotropy of the crystal growth rate,

nanowires of $CuInSe_2$ have been synthesized by using templates or metal nanocrystal as the catalytic seed.[73, 89, 94, 100-103] The reactions with well-passivating surfactants, such as oleylamine and alkanethiols, usually give small spherical or faceted nanocrystals.[83, 87, 104] However, formation of anisotropic nanocrystals of $CuInSe_2$, such as hexagonal microplates, without the use of catalysts or templates has also been reported indicating anisotropic crystal growth is possible although it may be weak.[83, 105-107] As mentioned in the Introduction section, when different facets of the crystals do not have sufficient intrinsic anisotropy, surfactants with weaker binding affinity may reveal the differences between facets more readily than the surfactants with the stronger binding affinity. Based on this reasoning, we performed a comparative study to test whether reducing the amount of a strongly binding surfactant in the synthesis can enhance the anisotropic growth of $CuInSe_2$ nanocrystals.

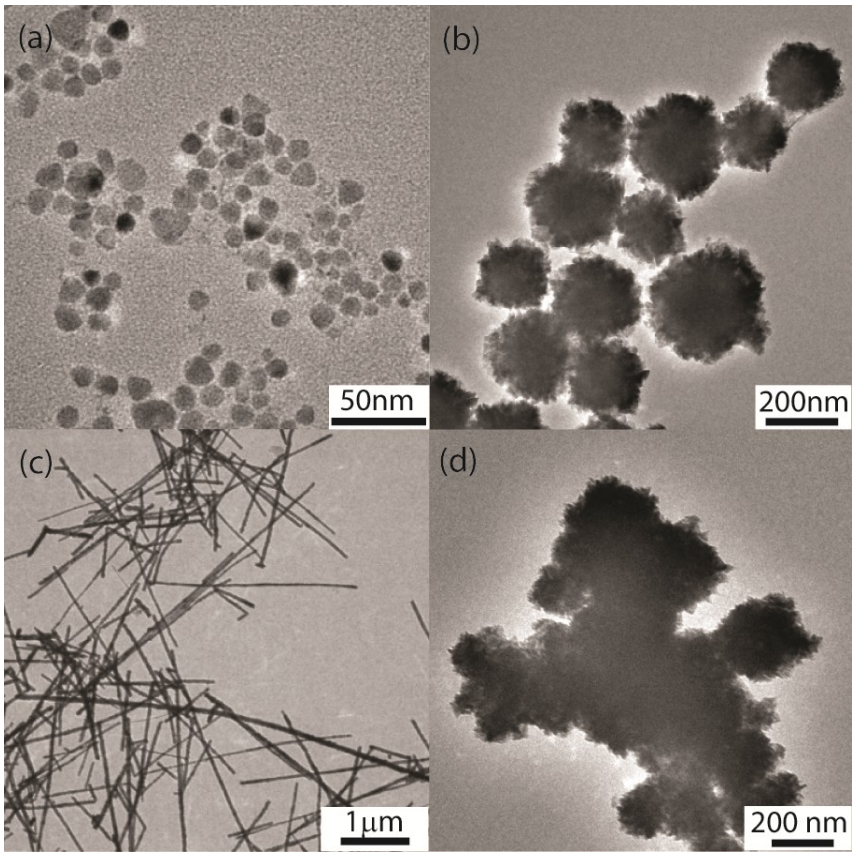

Figure 5.2. TEM images of $CuInSe_2$ nanocrystals prepared under the reaction conditions of Table 1. (a) small nanospheres, (b) large nanospheres, (c) nanowires and (d) aggregates.

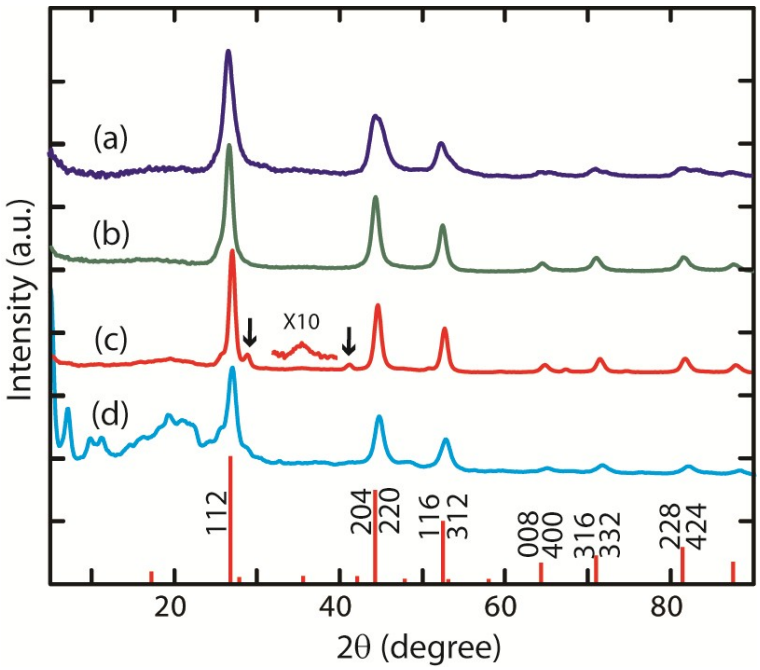

Figure 5.3. XRD patterns of (a) small spheres, (b) large spheres, (c) nanowires with magnified region around 35.5° and (d) aggregates. Red vertical lines indicate the peak positions for bulk phase of $CuInSe_2$.

Figure 5.2(a) to (d) compares the morphologies of $CuInSe_2$ nanocrystals synthesized with different combinations of surfactant and solvent as summarized in Table 5.1. Chloride salts of Cu and In were mainly used as metal precursors, except $Cu(acac)_2$ used to synthesize the small spheres. Se powder dissolved in either TOP or oleylamine was used as the Se precursor. The amount of oleylamine, a strongly binding surfactant, was varied in decreasing order from (a) to (d). Figure 5.3 shows the X-ray diffraction (XRD) patterns of the nanocrystals shown in Figure 5.2. All four nanocrystal samples show the same major peaks attributable to

chalcopyrite structure of $CuInSe_2$.[115] While the chalcopyrite and sphalerite phases have similar crystal structures, chalcopyrite can be identified by minor peaks such as a peak around 35.5°.[83] A magnified view of the XRD pattern in curve (c) of Figure 5.3 shows this minor peak attributable to the chalcopyrite structure. The XRD pattern of the nanowires exhibits other minor peaks (marked with arrows) attributed to Cu_3Se_2, which has been previously observed as an impurity in SLS-grown $CuInSe_2$ nanowires. Energy dispersive X-ray (EDX) measurements of the samples indicated that the composition of the nanocrystals are close to the stoichiometric ratio but slightly rich in Se by ~<5%. The purity of the phase and crystal structures at different compositions of Cu-In-Se ternary system has been previously addressed in a number of earlier works.[84, 116-118] Here, we will focus primarily on the comparison of the average structures and morphologies of the nanocrystals prepared under different surfactant/solvent environments.

Small spherical nanocrystals (diameter <10 nm) were formed when only oleylamine was present as the solvent and surfactant as shown in Figure 5.2(a). This observation is consistent with the results from earlier works, where small $CuInSe_2$ nanocrystals with relatively isotropic morphologies were synthesized in the presence of a strongly binding surfactant such as amine.[104] Figure 5.2(b) shows the nanocrystals synthesized in the mixture of oleylamine, TOP and TOPO, where the fraction of oleylamine in the solvent/surfactant mixture was reduced compared to the case of Figure 5.2(a). With the decrease in the fraction of oleylamine, the size of the nanocrystals became generally larger with comparable reaction times. A high

resolution TEM image of the large sphere, Figure 5.4, indicates that this structure is most likely formed via disordered agglomeration of the smaller faceted units rather than ordered attachment of the individual building blocks.

When oleylamine was completely removed and only TOPO and TOP were present in the solvent/surfactant mixture, we obtained nanocrystals of two very different morphologies. In one case, nanowires of tens of nanometers in width and several microns in length were formed as shown in Figure 5.2(c). On the other hand, highly aggregated nanocrystals without well-defined morphologies were also formed as shown in Figure 5.2(d). The large aggregates were obtained under the identical reaction conditions that produced the nanowires. Such radical differences in the morphologies of the nanocrystals synthesized under apparently the same conditions were found to be due to dioctylphosphine oxide (DOPO), which was present as an impurity in the particular batch of TOPO used under the reaction condition (c). In fact, DOPO is considered to play the key role in forming nanowires of $CuInSe_2$ in this study as will be discussed later. DOPO is a weaker surfactant than oleylamine and seems to promote the anisotropic growth of $CuInSe_2$ nanocrystals more readily than oleylamine, which is consistent with our earlier hypothesis. Further discussion on the identification of DOPO as the key surfactant and its role in the synthesis of $CuInSe_2$ nanowires will be made in the following sections.

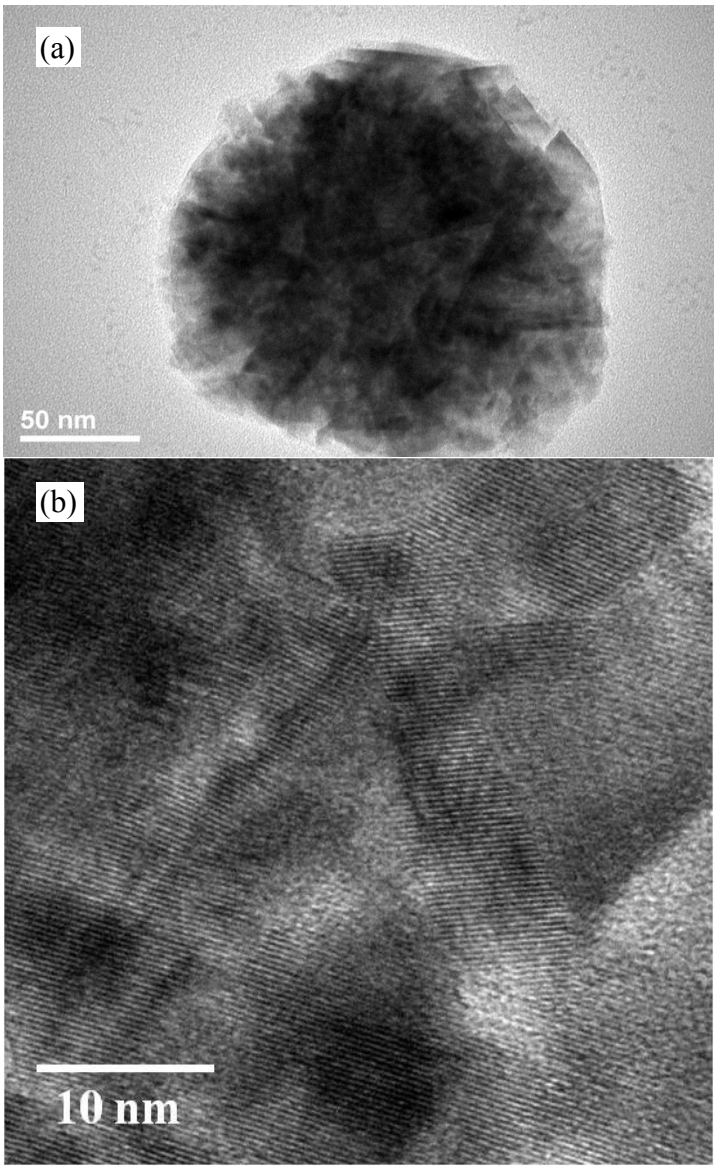

Figure 5.4. (a) A single large $CuInSe_2$ nanosphere with (b) corresponding high resolution TEM image of large $CuInSe_2$ nanospheres.

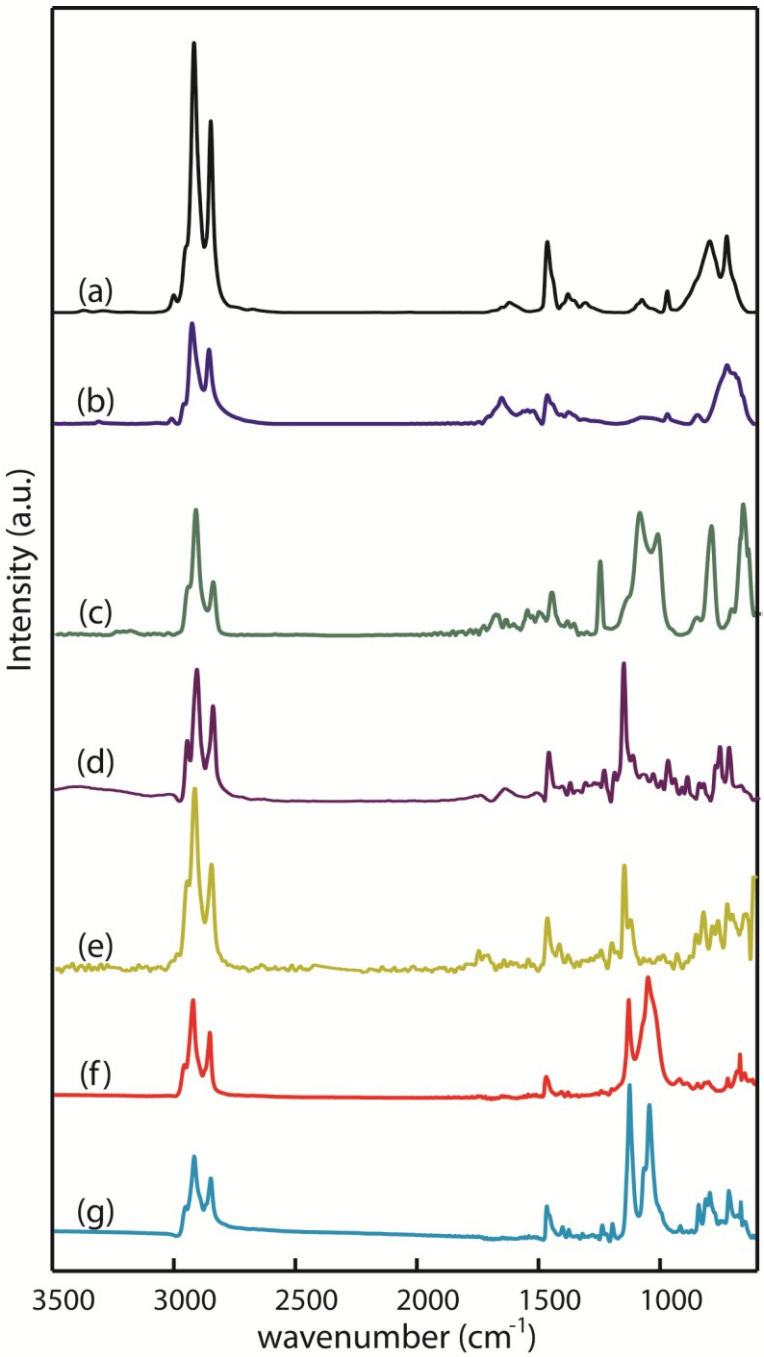

Figure 5.5. FT-IR spectra of (a) oleylamine (b) small spheres (c) large spheres, (d) DOPO, (e) TOPO, (f) nanowires and (g) large aggregates. The arrows indicate the peaks corresponding to the functional groups present in the surfactants.

5.2.2 Identification of surfactant molecules on the nanocrystal surface

In order to verify whether the different morphologies of $CuInSe_2$ nanocrystals shown in Figure 5.2 correlate with the surfactant used, we attempted to identify the surfactant molecules passivating the surface of the nanocrystals. For this purpose, infrared (IR) absorption spectroscopy and mass spectrometry were used. IR absorption spectra of thoroughly rinsed $CuInSe_2$ nanocrystals with different morphologies and pure surfactant are shown in Figure 5.5. An IR spectrum, Figure 5.5 (b), obtained from the small spherical nanocrystals exhibits a band attributed to the C=C stretching mode at 1652 cm^{-1} and N-H bending (scissoring) mode at 1560 cm^{-1} indicating that oleylamine is passivating the surface.[119-121] IR spectra from the nanocrystals of Figure 5.2(c) and (d) (nanowires and large aggregates) exhibit peaks attributed to P-O stretching modes near 1125 and 1045 cm^{-1} suggesting the presence of a phosphine oxide group coordinated to both, Cu^{+} and In^{3+} ions.[122] The IR spectrum from the large spherical nanocrystals, Figure 5.2(b), has peaks that can be assigned to both amine and phosphine oxide groups, consistent with the reaction condition containing both oleylamine and TOPO.

The pure solvent IR spectra are shown on Figure 5.5 (a), (d) and (e). Pure TOPO and DOPO only have one P-O stretching modes at 1142 and 1155 cm^{-1}, respectively, but due to the phosphine oxide potentially being bound to two different cations, the splitting of the stretching mode could be explained by this. The finger print region of the spectra is of interest as well. This region would give

some insight as to how the surfactant is bound to the nanoparticles. While there is very little similarity in the finger print region from sample to sample or even compared to the pure surfactant, theoretical modeling and calculations of the metal surfactants bonding could be performed to gain a better understanding.

The IR data could not explain the difference in morphology of the samples shown in Figure 5.2(c) and (d) as it would seem they are passivated by the same molecule. So, to more clearly identify the surfactant molecules on the surface of the samples shown in Figure 5.2(c) and (d), the mass spectra of the surfactant molecules recovered from the surface of the thoroughly rinsed nanocrystal samples were obtained. Initially, the nanocrystal samples rinsed with ethanol multiple times were digested in 0.1% formic acid solution in the mixture of acetonitrile and water (each 50% by volume). The supernatant recovered from the solution was analyzed with ESI mass spectrometry. Figure 5.6(a) and (b) show the mass spectra of the recovered supernatants from the nanowires and aggregates of $CuInSe_2$ respectively. The mass spectra show both TOPO (m/z=387.4, $[TOPO+H]^+$) and a known impurity of TOPO, DOPO (m/z=313.3, $[DOPO+K]^+$).[113] The skeletal structures of TOPO and DOPO are illustrated in Figure 5.7. DOPO has one less eight carbon alkyl chain compared to TOPO.

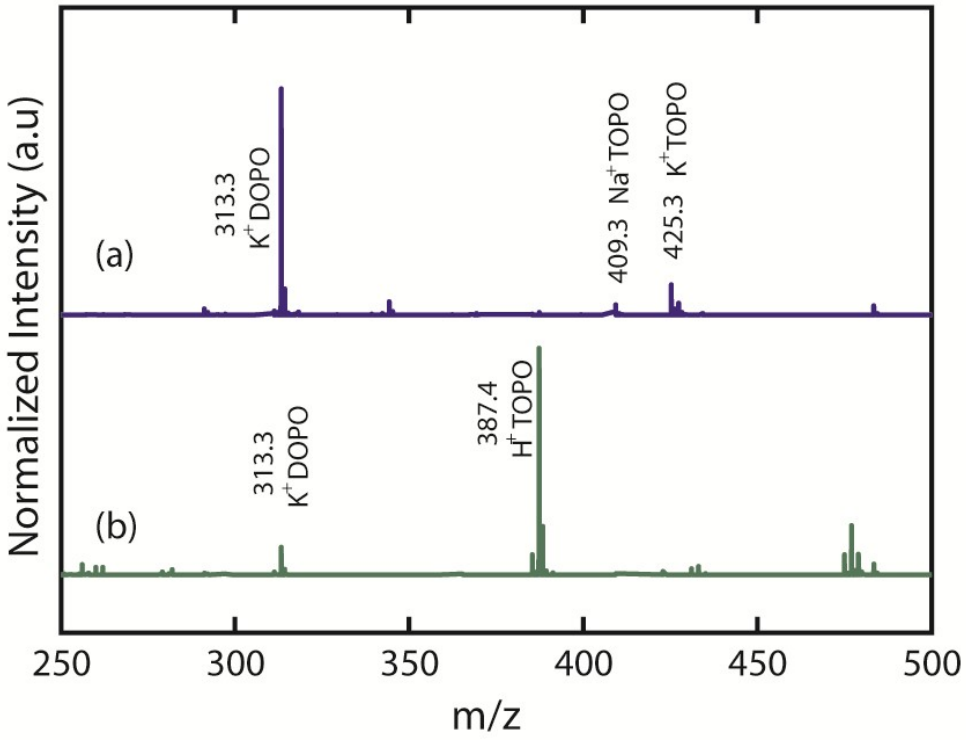

Figure 5.6. ESI-MS of $CuInSe_2$ (a) nanowires and (b) large aggregates.

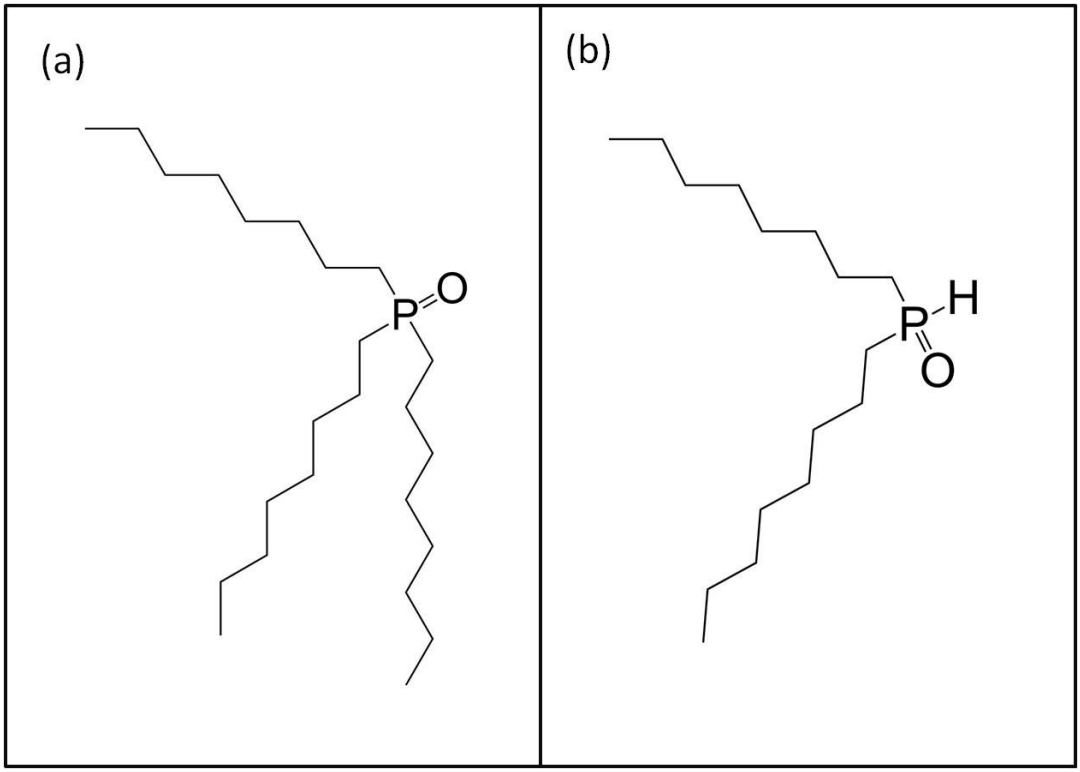

Figure 5.7. (a) Skeletal structure of trioctylphosphine oxide (TOPO) and dioctylphosphine oxide (DOPO).

In order to further verify the role of DOPO in the formation of $CuInSe_2$ nanowires, we compared the morphologies of the nanocrystals synthesized with different proportions of DOPO to TOPO. For this purpose, we synthesized DOPO following the procedure described in the experimental section. The purities of DOPO and TOPO used for this comparative study were checked by ESI mass spectrometry. DOPO was found to be >97% pure with small unidentifiable impurity peaks using ESI-MS. ^{31}P NMR spectra showed no sign of other phosphorous impurities. ^{31}P NMR of TOPO (Strem, >99%) showed no indication of contamination by DOPO. The reactions were carried out in the surfactant and solvent mixtures of four different compositions (mass ratio): (a) TOPO only, (b) DOPO/TOPO=0.11, (c) DOPO/TOPO=0.67, (d) DOPO/octadecene=0.67. Composition (d), where TOPO was replaced with non-coordinating hydrocarbon (octadecene, ODE), was tested to further confirm the role of DOPO in forming the nanowires.

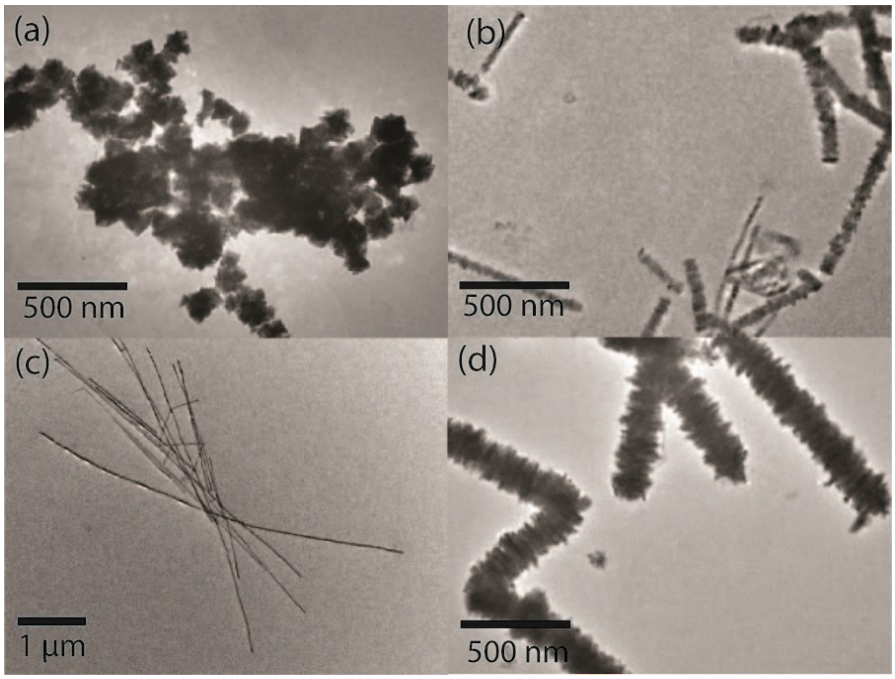

Figure 5.8. TEM images of $CuInSe_2$ in different reaction conditions corresponding to (a) TOPO only, (b) DOPO/TOPO=.11, (c) DOPO/TOPO=.67, (d) DOPO/ODE=.67.

Figure 5.8 compares the morphologies of the nanocrystals synthesized in four different compositions of surfactant and solvent mixtures described above. Only highly aggregated nanocrystals were obtained with >99% TOPO as the sole solvent and surfactant. Nanowires were formed when DOPO was added to the solvent mixture. The width of the nanowires decreased with increasing amount of DOPO as can be seen in Figure 5.8(b) and (c). The average width of the nanowires decreased with increasing amount of DOPO as can be seen in Figure 5.8(b) and (c) from 56nm to 29nm respectively. In addition, the standard deviation of the width of the wires also decreases by about 25%, with Figure 5.8(b) and (c) having a 42% and 17% deviation respectively (roughly 50 nanowires were counted from each batch). Nanowires could be formed even when TOPO was replaced with ODE that does not possess any coordinating capability, while the nanowires were much thicker than those obtained in the mixture of DOPO and TOPO. Mass spectra of the surfactants recovered from all the nanowires showed DOPO as the main component. These observations strongly indicate that DOPO is the key surfactant responsible for the formation of nanowires of $CuInSe_2$. The fact that TOPO is seen as a minor component in the mass spectra of nanowires and that the replacement of TOPO with ODE results in thicker nanowires suggests that TOPO also passivates the surface of the nanocrystal although to a less degree than DOPO.

It is intriguing that DOPO is strongly preferred over TOPO on the surface of $CuInSe_2$ nanowires despite the fact that both surfactants have the same functional group. The phosphine oxide group is considered to bind to cations on the surface of

various semiconductor nanocrystals.[123, 124] In fact, one might expect that TOPO would bind more strongly on the nanocrystal surface than DOPO since TOPO has one more alkyl group that is more electron-donating than a hydrogen atom. Therefore, the argument based on comparison of the coordinating capability of the functional group alone may not explain the observation. On the other hand, DOPO will experience less steric hindrance from the carbon chains than TOPO on the surface of the nanocrystals. The smaller steric hindrance may be the reason why DOPO is preferentially found on the surface of $CuInSe_2$ nanowire. This observation is also consistent with the earlier first-principle calculation study on the growth of CdSe nanorods, where the less bulky surfactant preferred the anisotropic growth more.[125]

5.2.3 Structure of $CuInSe_2$ nanowires

In order to obtain more detailed structural information on $CuInSe_2$ nanowires, selected-area electron diffraction (SAED) and high-resolution TEM (HRTEM) measurements were made. Figure 5.9(a) to (d) show a TEM image of a representative nanowire and SAED patterns obtained from the circled regions along the nanowire. The wire growth direction is identified as normal to the (112) planes (d_{112} = 0.33 nm). Since the selected areas contain multiple (112) nano-twins, the diffraction spots split along this $(112)^*$ reciprocal direction. Figure 5.10(a) and (b) show the TEM images of the nanowires obtained at higher resolution. HRTEM images of two different regions of the nanowire indicated in Figure 5.10(b) are

displayed in Figure 5.10(c) and (d). These two regions exhibit a twinning relationship around the growth axis with ~60° rotation about the common (112) plane. A previous study has shown that twinning in chalcopyrite $CuInSe_2$ occurs at (112) planes.[126] The indexed electron diffraction patterns and the lattice fringe patterns in HRTEM images confirm that the nanowires grow perpendicular to the (112) planes. The same growth direction was also observed in Wooten et al.'s work employing SLS growth and Au/Bi nanocrystal catalyst.[100]

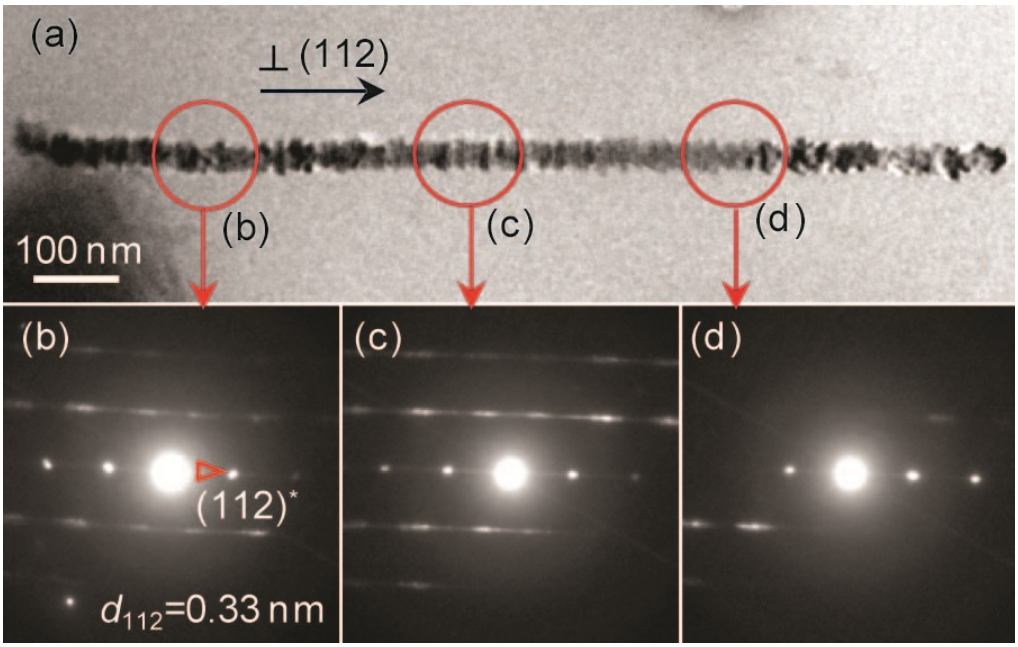

Figure 5.9. TEM image of (a) a nanowire, and (b-d) SAED patterns of the nanowire in the circled regions in (a).

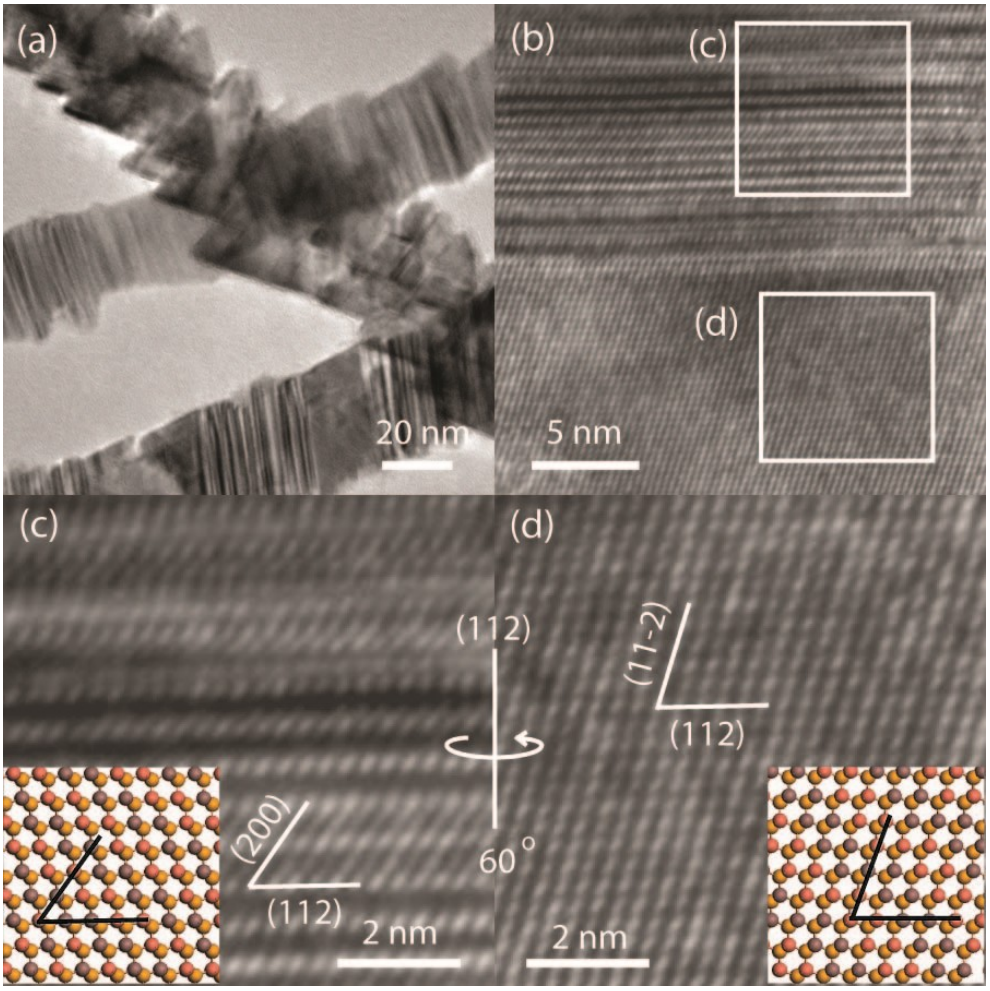

Figure 5.10. (a-b) Representative TEM images of nanowires. (c-d) HRTEM images from the areas indicated in (b). Insets of (c-d) are theoretically modeled using material studio.[127]

$CuInSe_2$ nanowires prepared in our study exhibit generally rougher surfaces than those prepared from VLS or SLS growth methods. It is interesting to note that many of the nanowires show a saw-tooth like surface along the growth axis. In some cases, a contour of stacked truncated tetrahedra can be clearly observed, e.g. in Figure 5.10(a), that gives rise to the regular saw-tooth pattern on the surface.

In order to examine the morphology of the nanowires in more detail, scanning transmission electron microscopy (STEM) images and a 3-D tomogram reconstructed from a series of angle-resolved TEM images were obtained. Figure 5.11(a) shows a STEM *Z*-contrast image of a nanowire with saw-toothed surface, which clearly shows the triangular shapes stacked along the nanowires. Cross sectional views at two selected positions indicated in Figure 5.11(b) are also shown in Figure 5.11(c) and (d). A single triangle or two superposed triangles are clearly identified. The orientational relationship between the cross sections shown in Figure 5.11(c) and (d) clearly indicates the twinning with ~60° rotation consistent with the twinning of the lattice observed in HRTEM images of the nanowires in Figure 5.10. While moving along the growth axis of the nanowire, all the identifiable triangular cross sections were oriented in the same or ~60°-rotated directions, Figure 5.12. These observations indicate that the morphology of the nanowire can be viewed as a stack of truncated tetrahedra with occasional rotations of a tetrahedron unit by ~60° around the growth axis.

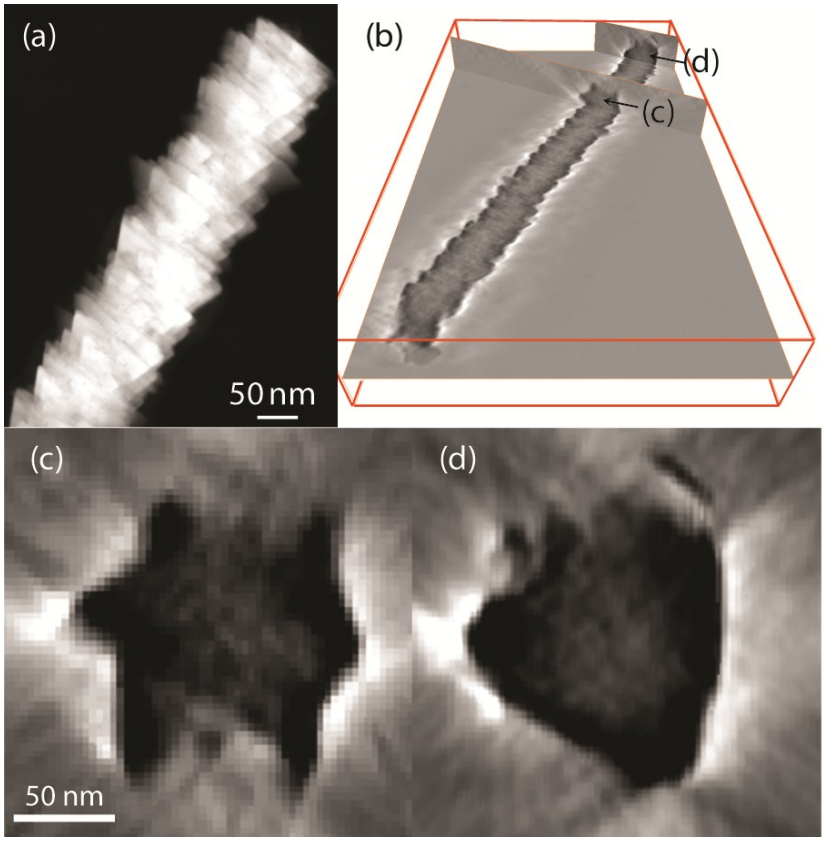

Figure 5.11. (a) STEM image of a nanowire, (b) two locations of nanowires where cross sectional views are obtained, (c-d) cross sectional view of nanowires obtained from reconstructed 3-dimensional tomogram at two locations shown in (b).

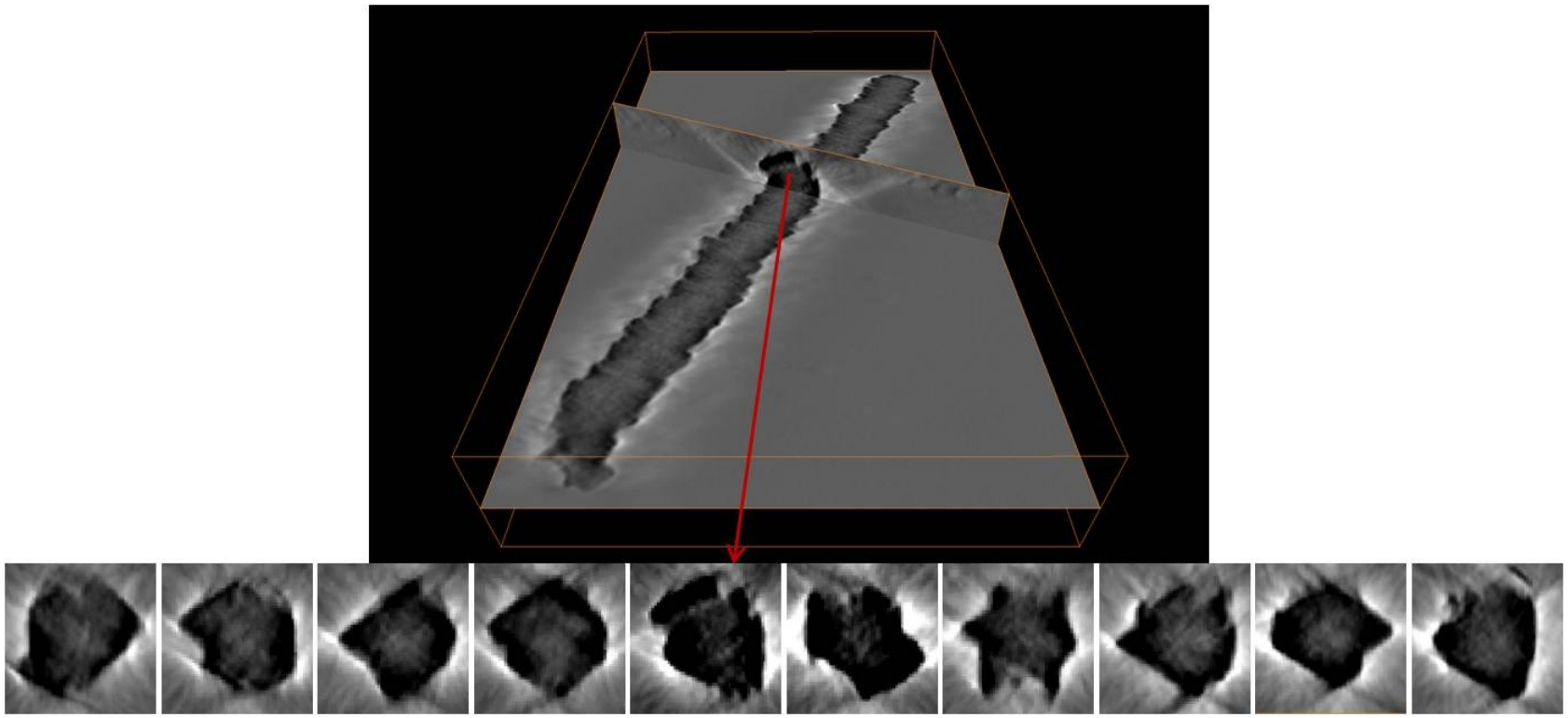

Figure 5.12 Single nanowire with multiple cross sectional views.

5.2.4 Growth mechanism

In principle, $CuInSe_2$ nanowires can form in a number of different ways under our experimental condition. One possible mechanism is oriented attachment of small tetrahedron units of $CuInSe_2$. Formation of nanowires from smaller building blocks via dipolar interaction between the building blocks has been previously observed in a number of nanocrystals with cubic symmetry, such as PbSe nanocubes.[8] Since the lattice structure of $CuInSe_2$ is double zinc-blende, nanocrystals of tetrahedron morphology can be formed, which can be a potential building block.[86] The second possibility is SLS growth, analogues to Wooten et al.'s work. While we did not add any metal nanocrystals as the catalytic seed, there is a possibility that metal nanocrystals form in-situ and function as the catalytic seed. In our reaction, it would most likely be the metallic indium, which is previously known to catalyze nanowire growth of GaAs, Si, InAs and InP.[128-130] Finally, $CuInSe_2$ nanowires can form simply via anisotropic passivation of different facet during the growth in the solution.

We ruled out the possibility of oriented attachment of tetrahedron building blocks for the following reasons. Firstly, TEM images of the aliquots taken at different times during the reaction did not show any signature of individual nanocrystal building blocks, while longer reaction time generally resulted in the growth of longer and thicker nanowires. Figure 5.13(a) to (c) show the morphology of nanowires at the reaction time of from 1, 1.5 and 3 hours respectively, when the reaction was performed with DOPO/TOPO mass ratio of 0.67. The electron

diffraction patterns that correspond to Figure 5.13 are shown in Figure 5.14. It can be seen that the growth axis of parallel to (112) is maintained from the beginning of the nanowire growth. Furthermore, formation of nanowires from the attachment of tetrahedron units requires face-to-apex attachment for the whole length of the nanowire, which is not a very probable event. A more likely scenario is the facet-to-facet attachment of tetrahedron units, which would not lead to the linear nanowire structure.

In order to check whether metallic indium is formed at any stage of the reaction and function as the catalytic seed for SLS growth, aliquots taken at different times during the reaction were analyzed with XRD. At any stages of reaction, no signature of metallic indium could be found under our reaction condition in XRD patterns. EDX line scan was also performed along the growth axis at several regions including the both ends of the nanowire to identify potentially indium-rich region that may indicate the presence of metallic indium seed, Figure 5.15 to Figure 5.17. Figure 5.15(a) and (b) show the regions of EDX line scan and the corresponding elemental compositions. All three regions exhibit the nearly identical composition showing no indication of metallic indium catalytic seed. Figure 5.16 and 5.17 support this conclusion. According to the earlier studies on the synthesis of indium nanocrystals, both high temperature (e.g. 360 °C) and highly reducing reagents (e.g. Na metal) are required to reduce $InCl_3$ to metallic indium. The absence of metallic indium in our reaction may be due to insufficiently reducing condition to produce In^0 from $InCl_3$.[131]

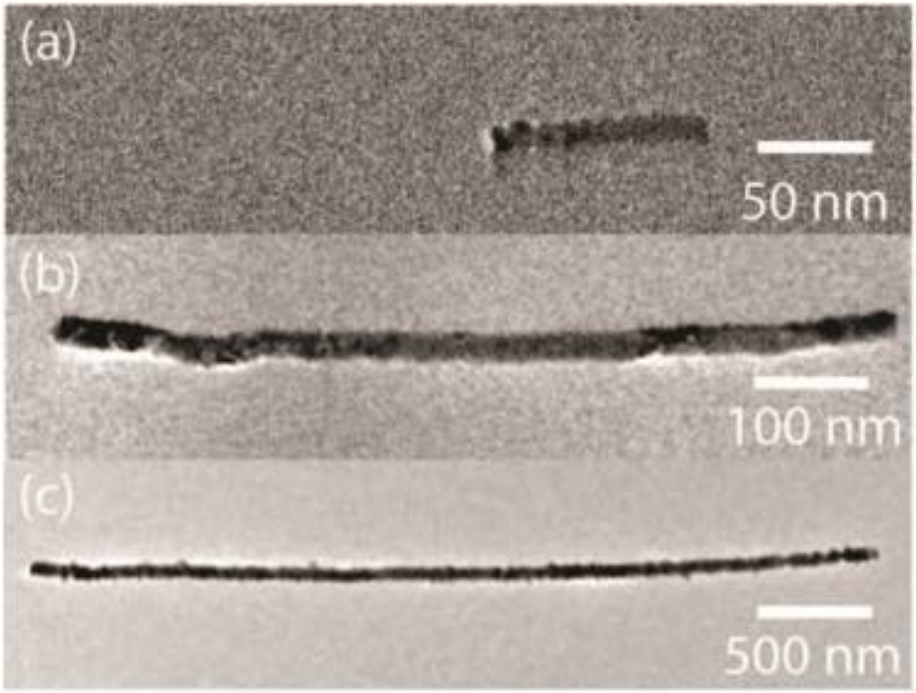

Figure 5.13. TEM images of nanowire with at different growth times: (a) 1 hour, (b) 1.5 hours and (c) 3 hours.

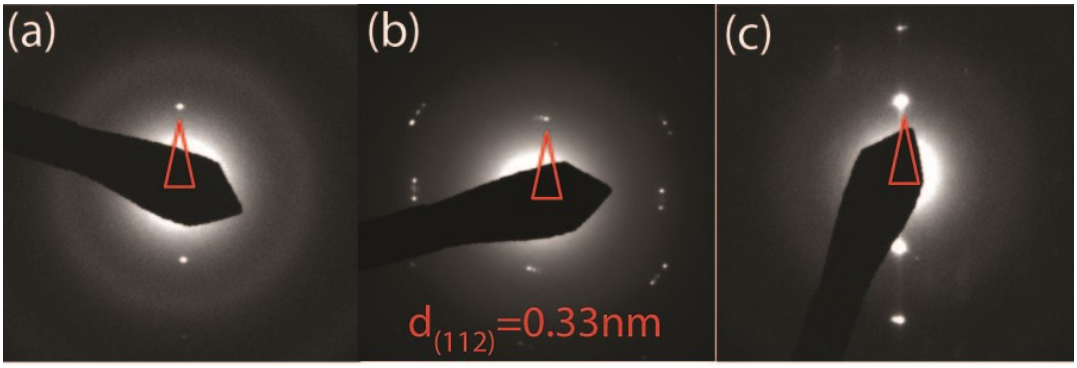

Figure 5.14. Electron diffraction patterns corresponding to Figure 5.15(a-c). Diffraction spots corresponding to the (112) planes have been indexed and are shown by the red arrow.

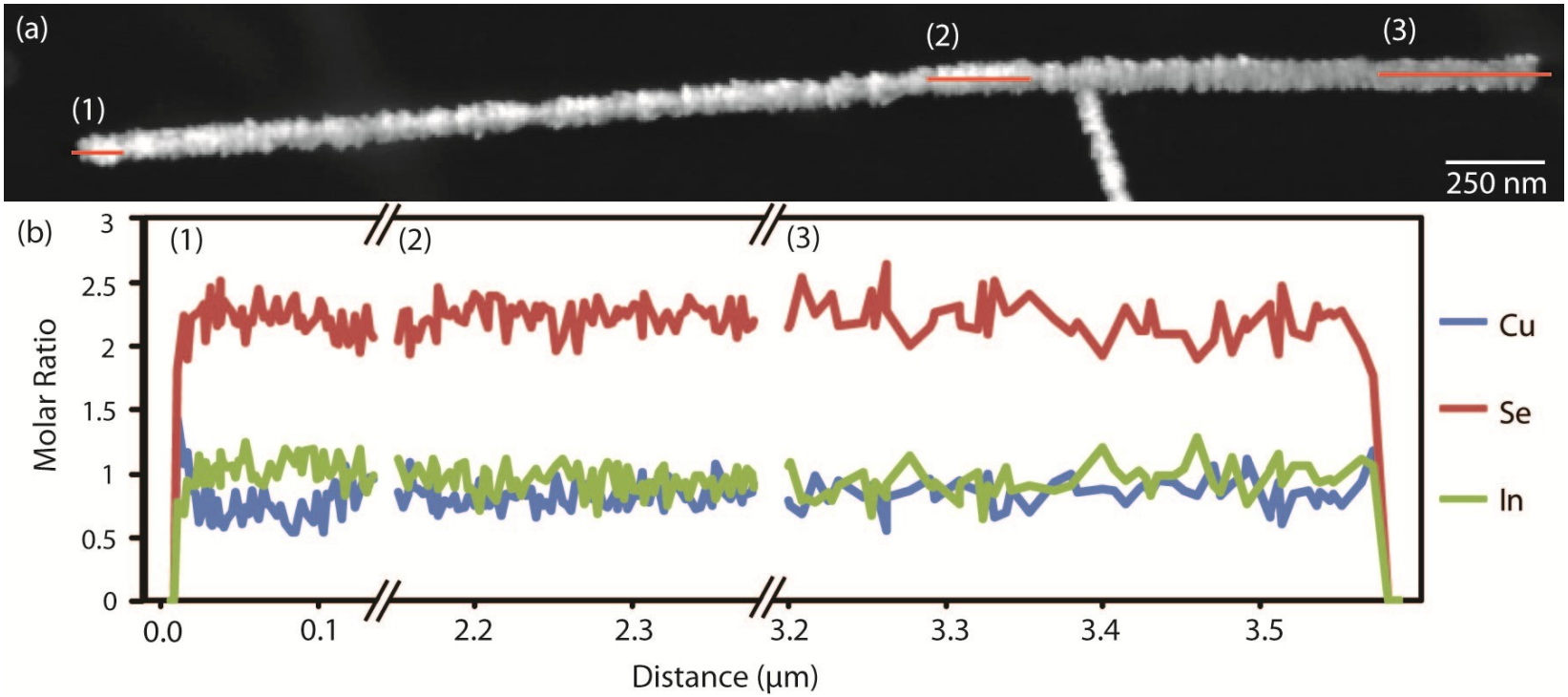

Figure 5.15. (a) STEM image of a nanowire with three red lines corresponding to the location of the EDX line scan. (b) The resulting line scans are shown and correspond to the labeled lines (1-3) on the STEM image.

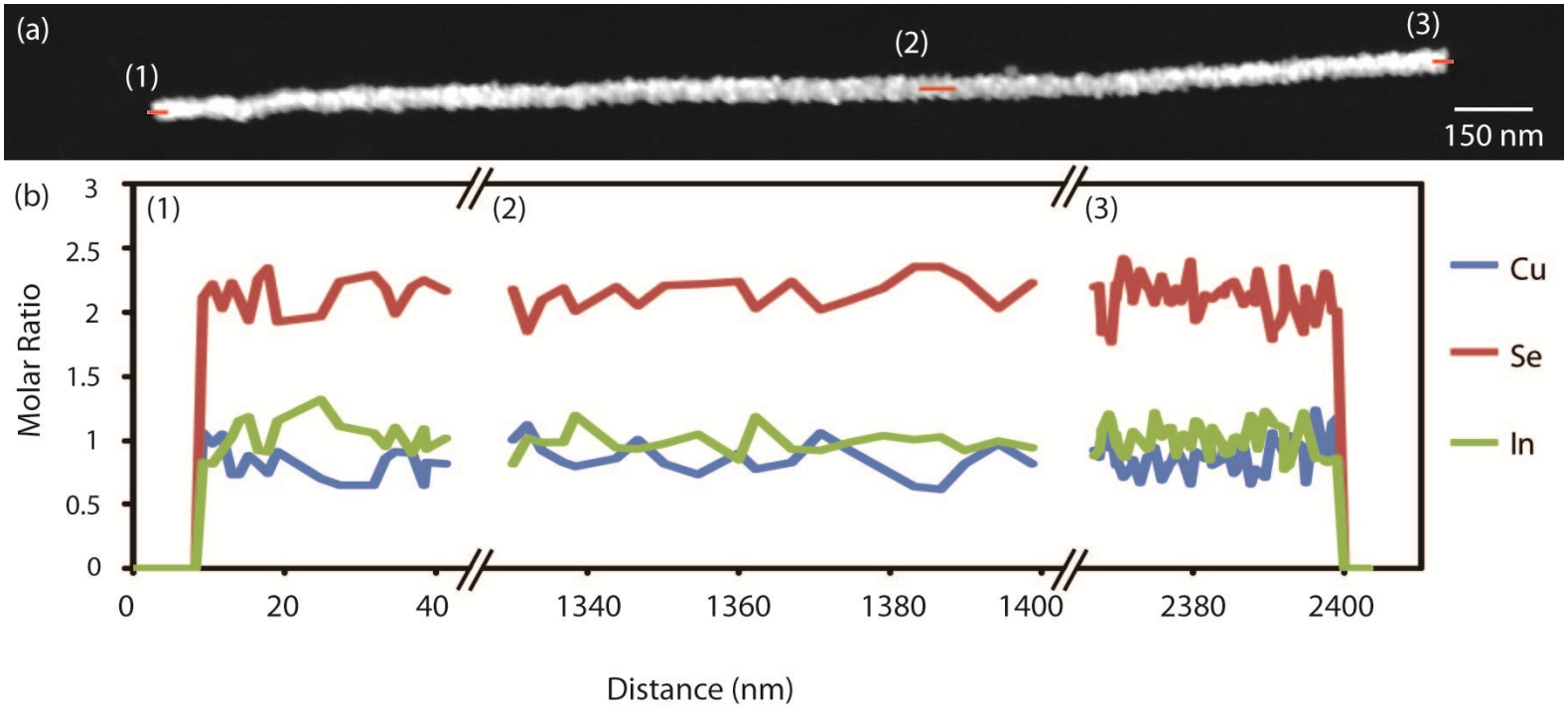

Figure 5.16. (a) STEM image of a nanowire with three red lines corresponding to the location of the EDX line scan. (b) The resulting line scans are shown and correspond to the labeled lines (1-3) on the STEM image.

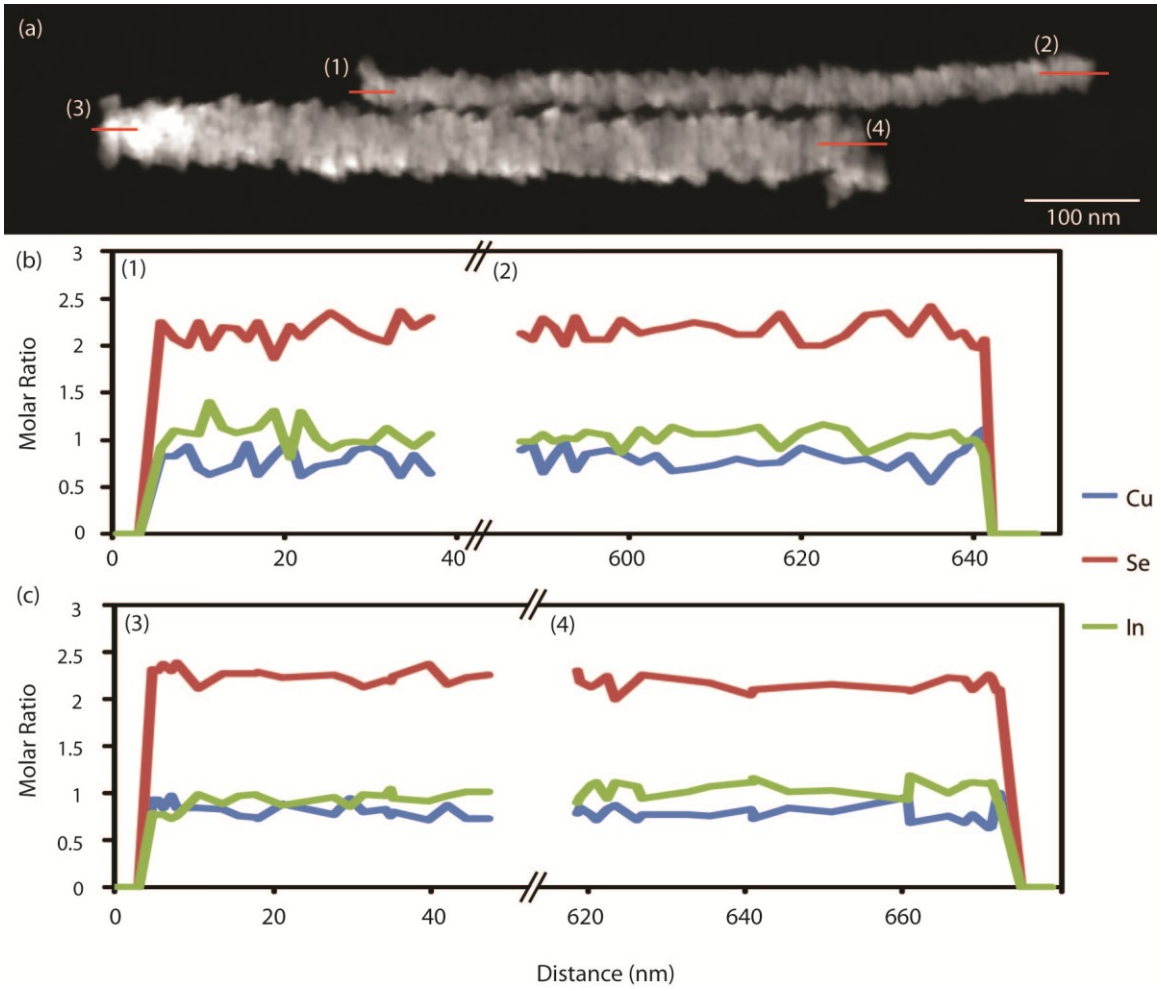

Figure 5.17. (a) STEM image of two nanowires. Each nanowire has red lines that correspond to the location of the EDX line scans. (b-c) The resulting line scans are shown and correspond to the labeled lines (1-4) on the STEM image.

Therefore, a more plausible route for the formation of $CuInSe_2$ nanowires in this study is continuous anisotropic growth assisted by the anisotropic surface passivation by weak surfactant molecules. Figure 5.13, showing the time sequence of the morphologies, also suggests that the nanowire is growing continuously both in length and width. The growth of nanowires in the direction normal to (112) plane may be due to the differences in the polarity of (112) plane forming the base of tetrahedron and three {114} planes.[86] The growth of nanowires in the direction normal to (112) plane may be due to the differences in the polarity of (112) plane forming the base of tetrahedron and three {114} planes. The (112) plane, composed entirely of either all metal or selenium ions, may be better passivated by DOPO than the other planes with both cations and anions resulting in anisotropic growth perpendicular to (112) plane. Further computational study on the relative affinity of DOPO and TOPO on different facets will shed an additional insight into the mechanism of the growth of $CuInSe_2$ nanowires.

5.3 Conclusions

Solution-phase synthesis of chalcopyrite $CuInSe_2$ nanowires without using metal nanocrystal catalyst has been demonstrated. The morphology of chalcopyrite $CuInSe_2$ nanoparticles can progress from an isotropic to a highly anisotropic shape by varying the composition of strongly or weakly binding surfactants passivating the surface of the nanocrystals. DOPO was found to be the key surfactant for the growth of $CuInSe_2$ nanowires. Detailed analysis of the nanowire structure indicates

that they grew normal to the (112) plane with twinning around the growth axis by ~60° rotation. The nanowires of $CuInSe_2$ synthesized in this study exhibit an interesting saw-tooth surface morphology resembling a stack of truncated tetrahedra.

CHAPTER VI

CONCLUSIONS

6.1 General conclusions

6.1.1 Use of cation exchange to make transition metal chalcogenides

Transition metal chalcogenides, specifically platinum and palladium chalcogenides, were made using a cation exchange reaction with cadmium chalcogenide nanoparticles as the starting template. Cadmium chalcogenide nanoparticles were chosen as the starting material due to the ease in controlling shape and size of the nanoparticles. Solvation and volume change of reaction were studied to set up a framework which would allow cation exchange to be extended to more chemical compositions. It was found that by modifying the solvation conditions of the cations, the equilibrium of the system could be changed. Three different solvation conditions were studied, including a mixed solvent system, a single solvent system with a complexing agent and a mixed solvent system with a complexing agent. It was found that the mixed solvent system with the complexing agent, condition (C), was the most efficient. Solvation condition (C) used DDAB to solvate the reactant cations (either platinum or palladium) in toluene while the product cations (cadmium) could then move to the aqueous phase.

The crystal structure of the product and reactant nanomaterials must also be taken into account to predict the conservation or lack thereof for morphology. Three different morphological changes were found to occur: morphology

conservation, void formation or fragmentation. The morphological changes were found to result from the size and shape of the template nanoparticles as well as the change in lattice structure.

6.1.2 Solution phase synthesis of $CuInSe_2$ nanowires

Morphology of $CuInSe_2$ nanoparticles could be tuned by varying the relative amounts of surfactants with different binding affinities. Strongly binding surfactants, such as oleylamine, lead to smaller, more isotropic shapes, whereas weaker binding phosphine oxides gave much larger structures and allowed for anisotropic growth. It was found that DOPO, a known impurity in TOPO, was actually the key surfactant for anisotropic growth of $CuInSe_2$ nanowires. The nanowires which were made in a solution phase synthesis seem to grow without the use of metal nanoparticle catalysts. It is believed that the difference in steric bulk between TOPO and DOPO leads to the nanowire formation. Due to less steric hindrance from DOPO, a higher packing density of the surfactant may occur on the nanocrystal surface.

The nanowires were analyzed and found to have a rough surface. They grew perpendicular to the (112) plane, were made up of truncated tetrahedrons and had twinning around the growth axis by ~60°. The growth of the nanowires appeared to be due to a continuous growth mechanism which showed no evidence of catalytic growth.

6.2 Future directions

6.2.1 Extending cation exchange reactions

The experiments in Chapter 3 set up a framework to understand different parameters in cation exchange reactions. The goal is to be able to use cation exchange as an easy way to modify composition so as to obtain nanoparticles which would otherwise be difficult or costly to make. In the previous experiments, cadmium chalcogenide nanoparticles were used as the starting material and template due to the well established synthetic procedures to make the nanoparticles; however, in the future, it would be useful to only use other starting nanoparticles, such as Zn or Cu chalcogenides, so as to eliminate the toxic cadmium waste. For the platinum and palladium chalcogenide nanoparticles that were made, the catalytic properties were studied using the Heck reaction in collaboration with the Connell group. The nanoparticles did not act as a catalyst for the Heck reaction, but the platinum and palladium chalcogenides may be useful for other catalytic reactions such as hydrogenation reactions, which would be interesting to study.[42]

Further study of other complexing agents, for example crown ethers, which will modify the solvation conditions, will be useful in order to make cation exchange more accessible to other systems. Katari et al found that the excess surfactants in the reaction solution can affect the kinetics of the reactions.[123] This knowledge may be useful to make more complicated compositions via cation exchange such as ternary or even quaternary chalcogenides. Using two simultaneous cation exchange reactions, for which the solvation conditions of the

cations has been selectively chosen, may allow for two cations to be exchanged for one. Another possible way to approach making ternary nanomaterials would be to using a partial cation exchange. As an example of a partial exchange, one could use Cu_2Se as the starting nanomaterial with a partial exchange of In cations. If the resulting nanoparticles could then be annealing in solution, a ternary phase may be accessible.

Another set of interesting experiments would be to study a ternary nanoparticle undergoing cation exchange. One of two things could happen. The first scenario would be that both cations in the ternary nanoparticle are exchanged leading to a binary phase product. The other scenario would be that one of the two cations in the ternary material will selectively exchange leading to another ternary material. By making more complicated compositions of nanoparticles through the use of cation exchange, the material properties of the ternary or quaternary nanoparticles could then be studied in greater detail, allowing for possible integration into devices due to the ease of synthesis.

6.2.2 Anisotropic growth in other ternary or quaternary chalcogenide materials

The knowledge gained from the solution phase synthesis of different morphologies of $CuInSe_2$ may lead to other ternary or quaternary chalcogenide synthetic routes. While the $CuInSe_2$ nanowires will most likely not be efficient for uses in solar cell devices because of their rough surface and polycrystalline

structure, they may be useful in other applications such as thermoelectric devices. It would be interesting to study the material properties of the rough nanowires to see how useful they could be. In addition, the understanding of how binding affinity affects ternary structures may lead to better synthetic procedures for quaternary chalcogenide materials. Quaternary chalcogenides are more difficult to make in solution seeing as there are four elements in which to balance the precursors' reactivity to make one single crystal phase material. To date, there have been numerous studies that look at $CuInGaSe_2$ or similar materials in thin films for the use in solar cell materials.[132, 133] The next step would then be to find an easy solution phase synthesis of high quality quaternary chalcogenide materials for use in potential applications.

REFERENCES

1. Parak, W. J.; Manna, L.; Simmel, F. C.; Gerion, D.; Alivisatos, A. P., Quantum dots. In *Nanoparticles: From Theory to Application*, Schmid, G., Ed. Wiley-VCH: Weinheim, Germany, 2010; pp 3-47.
2. Scholes, G. D., Controlling the optical properties of inorganic nanoparticles. *Adv. Funct. Mater.* **2008,** *18* (8), 1157-1172.
3. Goldstein, A. N.; Echer, C. M.; Alivisatos, A. P., Melting in semiconductor nanocrystals. *Science* **1992,** *256* (5062), 1425-1427.
4. Kumar, S.; Nann, T., Shape control of II-VI semiconductor nanomateriats. *Small* **2006,** *2* (3), 316-329.
5. Manna, L.; Scher, E. C.; Alivisatos, A. P., Shape control of colloidal semiconductor nanocrystals. *J. Cluster Sci.* **2002,** *13* (4), 521-532.
6. Nair, P. S.; Fritz, K. P.; Scholes, G. D., Evolutionary shape control during colloidal quantum-dot growth. *Small* **2007,** *3* (3), 481-487.
7. Peng, Z. A.; Peng, X., Formation of high-quality CdTe, CdSe, and CdS nanocrystals using CdO as precursor. *J. Am. Chem. Soc.* **2001,** *123* (1), 183-184.
8. Cho, K.-S.; Talapin, D. V.; Gaschler, W.; Murray, C. B., Designing PbSe nanowires and nanorings through oriented attachment of nanoparticles. *J. Am. Chem. Soc.* **2005,** *127* (19), 7140-7147.

9. Peng, X. G.; Manna, L.; Yang, W. D.; Wickham, J.; Scher, E.; Kadavanich, A.; Alivisatos, A. P., Shape control of CdSe nanocrystals. *Nature* **2000,** *404* (6773), 59-61.

10. Gao, J. H.; Gu, H. W.; Xu, B., Multifunctional magnetic nanoparticles: Design, synthesis, and biomedical applications. *Acc. Chem. Res.* **2009,** *42* (8), 1097-1107.

11. Kim, S.; Fisher, B.; Eisler, H. J.; Bawendi, M., Type-II quantum dots: CdTe/CdSe(core/shell) and CdSe/ZinTe(core/shell) heterostructures. *J. Am. Chem. Soc.* **2003,** *125* (38), 11466-11467.

12. Munoz, J. E.; Cervantes, J.; Esparza, R.; Rosas, G., Iron nanoparticles produced by high-energy ball milling. *J. Nanopart. Res.* **2007,** *9* (5), 945-950.

13. Koch, C. C.; Whittenberger, J. D., Mechanical milling/alloying of intermetallics. *Intermetallics* **1996,** *4* (5), 339-355.

14. Milani, P.; DeHeer, W. A., Improved pulsed laser vaporization source for production of intense beams of neutral and ionized clusters. *Rev. Sci. Instrum.* **1990,** *61* (7), 1835-1838.

15. de Dios, A. S.; Diaz-Garcia, M. E., Multifunctional nanoparticles: Analytical prospects. *Anal. Chim. Acta* **2010,** *666* (1-2), 1-22.

16. Carbone, L.; Cozzoli, P. D., Colloidal heterostructured nanocrystals: Synthesis and growth mechanisms. *Nano Today* **2010,** *5* (5), 449-493.

17. Fan, F. R.; Liu, D. Y.; Wu, Y. F.; Duan, S.; Xie, Z. X.; Jiang, Z. Y.; Tian, Z. Q., Epitaxial growth of heterogeneous metal nanocrystals: From gold nano-

octahedra to palladium and silver nanocubes. *J. Am. Chem. Soc.* **2008,** *130* (22), 6949–6951.

18. Habas, S. E.; Lee, H.; Radmilovic, V.; Somorjai, G. A.; Yang, P., Shaping binary metal nanocrystals through epitaxial seeded growth. *Nat. Mater.* **2007,** *6* (9), 692-697.
19. Shi, W. L.; Zeng, H.; Sahoo, Y.; Ohulchanskyy, T. Y.; Ding, Y.; Wang, Z. L.; Swihart, M.; Prasad, P. N., A general approach to binary and ternary hybrid nanocrystals. *Nano Lett.* **2006,** *6* (4), 875-881.
20. Yu, H.; Chen, M.; Rice, P. M.; Wang, S. X.; White, R. L.; Sun, S. H., Dumbbell-like bifunctional Au-Fe_3O_4 nanoparticles. *Nano Lett.* **2005,** *5* (2), 379-382.
21. Kwon, K. W.; Shim, M., gamma-Fe_2O_3/II-VI sulfide nanocrystal heterojunctions. *J. Am. Chem. Soc.* **2005,** *127* (29), 10269-10275.
22. Kwon, K. W.; Lee, B. H.; Shim, M., Structural evolution in metal oxide/semiconductor colloidal nanocrystal heterostructures. *Chem. Mater.* **2006,** *18* (26), 6357-6363.
23. Gu, H. W.; Zheng, R. K.; Zhang, X. X.; Xu, B., Facile one-pot synthesis of bifunctional heterodimers of nanoparticles: A conjugate of quantum dot and magnetic nanoparticles. *J. Am. Chem. Soc.* **2004,** *126* (18), 5664-5665.
24. Pacholski, C.; Kornowski, A.; Weller, H., Site-specific photodeposition of silver on ZnO nanorods. *Angew. Chem.* **2004,** *43* (36), 4774-4777.

25. Carbone, L.; Kudera, S.; Giannini, C.; Ciccarella, G.; Cingolani, R.; Cozzoli, P. D.; Manna, L., Selective reactions on the tips of colloidal semiconductor nanorods. *J. Mater. Chem.* **2006,** *16* (40), 3952-3956.

26. Kudera, S.; Carbone, L.; Casula, M. F.; Cingolani, R.; Falqui, A.; Snoeck, E.; Parak, W. J.; Manna, L., Selective growth of PbSe on one or both tips of colloidal semiconductor nanorods. *Nano Lett.* **2005,** *5* (3), 445-449.

27. Talapin, D. V.; Koeppe, R.; Gotzinger, S.; Kornowski, A.; Lupton, J. M.; Rogach, A. L.; Benson, O.; Feldmann, J.; Weller, H., Highly emissive colloidal CdSe/CdS heterostructures of mixed dimensionality. *Nano Lett.* **2003,** *3* (12), 1677-1681.

28. Zhu, W.; Wang, W.; Shi, J., A reverse cation-exchange route to hollow PbSe nanospheres evolving from Se/Ag2Se core/shell colloids. *J. Phys. Chem. B* **2006,** *110* (20), 9785-9790.

29. Milliron, D. J.; Hughes, S. M.; Cui, Y.; Manna, L.; Li, J. B.; Wang, L. W.; Alivisatos, A. P., Colloidal nanocrystal heterostructures with linear and branched topology. *Nature* **2004,** *430* (6996), 190-195.

30. Nadenau, V.; Braunger, D.; Hariskos, D.; Kaiser, M.; Koeble, C.; Oberacker, A.; Ruckh, M.; Ruehle, U.; Schaeffler, R., Solar cells based on $CuInSe_2$ and related compounds: Material and device properties and processing. *Prog. Photovoltaics* **1995,** *3* (6), 363-382.

31. Bari, R. H.; Patil, L. A.; Patil, P. P., Structural, optical and electrical properties of chemically deposited nonstoichiometric copper indium diselenide films. *Bull. Mater. Sci.* **2006,** *29* (5), 529-534.

32. Maikov, G. I.; Vaxenburg, R.; Sashchiuk, A.; Lifshitz, E., Composition-tunable optical properties of colloidal IV-VI quantum dots, composed of core/shell heterostructures with alloy components. *ACS Nano* **2010,** *4* (11), 6547-6556.

33. Bailey, R. E.; Nie, S. M., Alloyed semiconductor quantum dots: Tuning the optical properties without changing the particle size. *J. Am. Chem. Soc.* **2003,** *125* (23), 7100-7106.

34. Vasquez, Y.; Henkes, A. E.; Bauer, J. C.; Schaak, R. E., Nanocrystal conversion chemistry: A unified and materials-general strategy for the template-based synthesis of nanocrystalline solids. *J. Solid State Chem.* **2008,** *181* (7), 1509-1523.

35. Son, D. H.; Hughes, S. M.; Yin, Y.; Alivisatos, A. P., Cation exchange reactions in ionic nanocrystals. *Science* **2004,** *306* (5698), 1009-1012.

36. Wark, S. E.; Hsia, C. H.; Son, D. H., Effects of ion solvation and volume change of reaction on the equilibrium and morphology in cation-exchange reaction of nanocrystals. *J. Am. Chem. Soc.* **2008,** *130* (29), 9550-9555.

37. Jain, P. K.; Amirav, L.; Aloni, S.; Alivisatos, A. P., Nanoheterostructure cation exchange: Anionic framework conservation. *J. Am. Chem. Soc.* **2010,** *132* (29), 9997-9999.

38. Robinson, R. D.; Sadtler, B.; Demchenko, D. O.; Erdonmez, C. K.; Wang, L.-W.; Alivisatos, A. P., Spontaneous superlattice formation in nanorods through partial cation exchange. *Science* **2007,** *317* (5836), 355-358.

39. Chan, E. M.; Marcus, M. A.; Fakra, S.; El Naggar, M.; Mathies, R. A.; Alivisatos, A. P., Millisecond kinetics of nanocrystal cation exchange using microfluidic x-ray absorption spectroscopy. *J. Phys. Chem. A* **2007,** *111* (49), 12210-12215.

40. Jeong, U.; Camargo, P. H. C.; Lee, Y. H.; Xia, Y., Chemical transformation: a powerful route to metal chalcogenide nanowires. *J. Mater. Chem.* **2006,** *16* (40), 3893-3897.

41. Jeong, U.; Kim, J.-U.; Xia, Y.; Li, Z.-Y., Monodispersed spherical colloids of Se@CdSe: Synthesis and use as building blocks in fabricating photonic crystals. *Nano Lett.* **2005,** *5* (5), 937-942.

42. Dey, S.; Jain, V. K., Platinum group metal chalcogenides: their syntheses and applications in catalysis and materials science. *Platinum Met. Rev.* **2004,** *48* (1), 16-29.

43. Kuhn, B.; Kaefer, W.; Fess, K.; Friemelt, K.; Turner, C.; Wendl, M.; Bucher, E., Thermoelectric properties of $CuIn_{1-x}Ga_xTe_2$ single crystals. *Phys. Status Solidi A* **1997,** *162* (2), 661-671.

44. Lewerenz, H. J., Development of copper indium disulfide into a solar material. *Sol. Energy Mater. Sol. Cells* **2004,** *83* (4), 395-407.

45. Siebentritt, S., Wide gap chalcopyrites: Material properties and solar cells. *Thin Solid Films* **2002,** *403-404*, 1-8.

46. Henkes, A. E.; Vasquez, Y.; Schaak, R. E., Converting metals into phosphides: A general strategy for the synthesis of metal phosphide nanocrystals. *J. Am. Chem. Soc.* **2007,** *129* (7), 1896-1897.

47. Schaak, R. E.; Sra, A. K.; Leonard, B. M.; Cable, R. E.; Bauer, J. C.; Han, Y.-F.; Means, J.; Teizer, W.; Vasquez, Y.; Funck, E. S., Metallurgy in a beaker: Nanoparticle toolkit for the rapid low-temperature solution synthesis of functional multimetallic solid-state materials. *J. Am. Chem. Soc.* **2005,** *127* (10), 3506-3515.

48. Yin, Y.; Erdonmez, C. K.; Cabot, A.; Hughes, S.; Alivisatos, A. P., Colloidal synthesis of hollow cobalt sulfide nanocrystals. *Adv. Funct. Mater.* **2006,** *16* (11), 1389-1399.

49. Yin, Y.; Rioux, R. M.; Erdonmez, C. K.; Hughes, S.; Somorjai, G. A.; Alivisatos, A. P., Formation of hollow nanocrystals through the nanoscale kirkendall effect. *Science* **2004,** *304* (5671), 711-714.

50. Samal, A. K.; Pradeep, T., Pt_3Te_4 nanoparticles from tellurium nanowires. *Langmuir* **2010,** *26* (24), 19136-19141.

51. Chen, J.-H.; Tai, M.-F.; Chi, K.-M., Catalytic synthesis, characterization, and magnetic properties of iron phosphide nanowires. *J. Mater. Chem.* **2004,** *14* (3), 296-298.

52. Henkes, A. E.; Schaak, R. E., Trioctylphosphine: A general phosphorus source for the low-temperature conversion of metals into metal phosphides. *Chem. Mater.* **2007,** *19* (17), 4234-4242.

53. Khanna, P. K.; Jun, K.-W.; Hong, K. B.; Baeg, J.-O.; Mehrotra, G. K., Synthesis of indium phosphide nanoparticles via catalytic cleavage of phosphorus carbon bond in n-trioctylphosphine by indium. *Mater. Chem. Phys.* **2005,** *92* (1), 54-58.

54. Chiang, R.-K.; Chiang, R.-T., Formation of hollow Ni_2P nanoparticles based on the nanoscale kirkendall effect. *Inorg. Chem.* **2007,** *46* (2), 369-371.

55. Han, M. Y.; Huang, W.; Chew, C. H.; Gan, L. M.; Zhang, X. J.; Ji, W., Large nonlinear absorption in coated Ag2S/CdS nanoparticles by inverse microemulsion. *J. Phys. Chem. B* **1998,** *102* (11), 1884-1887.

56. Song, W.; Han, X. X.; Chen, L.; Yang, Y. M.; Tang, B.; Ji, W.; Ruan, W. D.; Xu, W. Q.; Zhao, B.; Ozaki, Y., Site-specific deposition of Ag nanoparticles on ZnO nanorod arrays via galvanic reduction and their SERS applications. *J. Raman Spectrosc.* **2010,** *41* (9), 907-913.

57. Camargo, P. H. C.; Lee, Y. H.; Jeong, U.; Zou, Z.; Xia, Y., Cation exchange: A simple and versatile route to inorganic colloidal spheres with the same size but different compositions and properties. *Langmuir* **2007,** *23* (6), 2985-2992.

58. Mokari, T.; Rothenberg, E.; Popov, I.; Costi, R.; Banin, U., Selective growth of metal tips onto semiconductor quantum rods and tetrapods. *Science* **2004,** *304* (5678), 1787-1790.

59. Dloczik, L.; Koenenkamp, R., Nanostructure transfer in semiconductors by ion exchange. *Nano Lett.* **2003,** *3* (5), 651-653.

60. Lokhande, C. D.; Gadave, K. M., A simple chemical method for conversion of Cds into Ag_2S and CdSe into Ag_2Se. *Mater. Chem. Phys.* **1993,** *36* (1-2), 119-123.

61. Ristova, M.; Ristov, M., XPS profile analysis on Cds thin film modified with Ag by an ion exchange. *Appl. Surf. Sci.* **2001,** *181* (1-2), 68-77.

62. Park, J.; Zheng, H.; Jun, Y. W.; Alivisatos, A. P., Hetero-epitaxial anion exchange yields single-crystalline hollow nanoparticles. *J. Am. Chem. Soc.* **2009,** *131* (39), 13943–13945.

63. Cao, H. L.; Qian, X. F.; Wang, C.; Ma, X. D.; Yin, J.; Zhu, Z. K., High symmetric 18-facet polyhedron nanocrystals of Cu_7S_4 with a hollow nanocage. *J. Am. Chem. Soc.* **2005,** *127* (46), 16024-16025.

64. Koktysh, D. S.; McBride, J. R.; Dixit, S. K.; Feldman, L. C.; Rosenthal, S. J., PbS/PbSe structures with core-shell type morphology synthesized from PbS nanocrystals. *Nanotechnology* **2007,** *18* (49), 495607/1-495607/4.

65. Weinstein, M.; Wolff, G. A.; Das, B. N., Growth of wurtzite- CdTe and sphalerite-type CdS single-crystal films. *Appl. Phys. Lett.* **1965,** *6* (4), 73-75.

66. Traill, R. J.; Boyle, R. W., Hawleyite, isometric cadmium sulfide, a new mineral. *Am. Mineral.* **1955,** *40*, 555-559.

67. Groenvold, F.; Haraldsen, H.; Kjekshus, A., On the sulfides, selenides, and tellurides of platinum. *Acta Chem. Scand.* **1960,** *14* (6), 1879-1893.

68. Geller, S., The crystal structure of $Pd_{17}Se_{15}$. *Acta Cryst.* **1962,** *15*, 713-721.

69. Villars, P., Ed., *ASM Alloy Phase Diagrams Center; http://www.asminternational.org/AsmEnterprise/APD, ASM International, Materials Park, OH,* **2006**.

70. Reiss, P.; Bleuse, J.; Pron, A., Highly luminescent CdSe/ZnSe core/shell nanocrystals of low size dispersion. *Nano Lett.* **2002,** *2* (7), 781-784.

71. Yu, W. W.; Peng, X., Formation of high-quality CdS and other II-VI semiconductor nanocrystals in noncoordinating solvents: Tunable reactivity of monomers. *Angew. Chem.* **2002,** *41* (13), 2368-2371.

72. Elliot, D. J.; Furlong, D. N.; Gengenbach, T. R.; Grieser, F.; Urquhart, R. S.; Hoffman, C. L.; Rabolt, J. F., Reactions of complex-ions of platinum and palladium in langmuir-blodgett-films of dimethyldioctadecylammonium chlorometallates. *Colloids Surf., A* **1995,** *103* (3), 207-219.

73. Peng, H.; Schoen, D. T.; Meister, S.; Zhang, X. F.; Cui, Y., Synthesis and phase transformation of In_2Se_3 and $CuInSe_2$ nanowires. *J. Am. Chem. Soc.* **2007,** *129* (1), 34-35.

74. Marcus, Y., Thermodynamics of solvation of ions. Part 5.—Gibbs free energy of hydration at 298.15 K. *J. Chem. Soc., Faraday Trans.* **1991,** *87* (18), 2995-2999.

75. Stanbery, B. J., Copper indium selenides and related materials for photovoltaic devices. *Crit. Rev. Solid State Mater. Sci.* **2002,** *27* (2), 73-117.

76. Kraus, W.; Nolze, G., POWDER CELL - a program for the representation and manipulation of crystal structures and calculation of the resulting X-ray powder patterns. *J. Appl. cryst.* **1996,** *29*, 301-302.

77. Dembowski, J.; Marosi, L.; Essig, M., Platinum disulfide by XPS. *Surface Science Spectra* **1993,** *2* (2), 133-137.

78. Dembowski, J.; Marosi, L.; Essig, M., Platinum sulfide by XPS. *Surface Science Spectra* **1993,** *2* (2), 104-108.

79. Elvy, S. B.; Williams, P. A.; Buckley, A. N., XPS evidence for the incongruent surface oxidation of minerals in the Pd-Te-Bi system. *Surf. Interface Anal.* **1996,** *24* (9), 641-646.

80. Volynsky, A. B.; Stakheev, A. Y.; Telegina, N. S.; Senin, V. G.; Kustov, L. M.; Wennrich, R., Low-temperature transformations of sodium sulfate and sodium selenite in the presence of pre-reduced palladium modifier in graphite furnaces for electrothermal atomic absorption spectrometry. *Spectrochim. Acta, Part B* **2001,** *56B* (8), 1387-1396.

81. Suh, Y. S.; Park, D. G.; Jang, S. A., Investigation of stress behaviors and mechanism of void formation in sputtered $TiSi_x$ films. *Thin Solid Films* **2004,** *450* (2), 341-345.

82. Okamoto, H., The pd-se (palladium-selenium) system. *J. Phase Equilib. Diffus.* **1992,** *13* (1), 69-72.

83. Guo, Q.; Kim, S. J.; Kar, M.; Shafarman, W. N.; Birkmire, R. W.; Stach, E. A.; Agrawal, R.; Hillhouse, H. W., Development of $CuInSe_2$ nanocrystal and nanoring inks for low-cost solar cells. *Nano Lett.* **2008,** *8* (9), 2982-2987.

84. Zhang, S. B.; Wei, S.-H.; Zunger, A.; Katayama-Yoshida, H., Defect physics of the $CuInSe_2$ chalcopyrite semiconductor. *Phys. Rev. B Condens. Matter Mater. Phys.* **1998,** *57* (16), 9642-9656.

85. Kemell, M.; Ritala, M.; Leskelae, M., Thin film deposition methods for $CuInSe_2$ solar cells. *Crit. Rev. Solid State Mater. Sci.* **2005,** *30* (1), 1-31.

86. Koo, B.; Patel, R. N.; Korgel, B. A., Synthesis of $CuInSe_2$ nanocrystals with trigonal pyramidal shape. *J. Am. Chem. Soc.* **2009,** *131* (9), 3134-3135.

87. Zhong, H.; Li, Y.; Ye, M.; Zhu, Z.; Zhou, Y.; Yang, C.; Li, Y., A facile route to synthesize chalcopyrite $CuInSe_2$ nanocrystals in non-coordinating solvent. *Nanotechnology* **2007,** *18* (2), 025602/1-025602/6.

88. Panthani, M. G.; Akhavan, V.; Goodfellow, B.; Schmidtke, J. P.; Dunn, L.; Dodabalapur, A.; Barbara, P. F.; Korgel, B. A., Synthesis of $CuInS_2$, $CuInSe_2$, and $Cu(In_xGa_{1-x})Se_2$ (CIGS) nanocrystal "inks" for printable photovoltaics. *J. Am. Chem. Soc.* **2008,** *130* (49), 16770-16777.

89. Xu, J.; Luan, C.-Y.; Tang, Y.-B.; Chen, X.; Zapien, J. A.; Zhang, W.-J.; Kwong, H.-L.; Meng, X.-M.; Lee, S.-T.; Lee, C.-S., Low-temperature synthesis of $CuInSe_2$ nanotube array on conducting glass substrates for solar cell application. *ACS Nano* **2010,** *4* (10), 6064-6070.

90. Yin, Y.; Alivisatos, A. P., Colloidal nanocrystal synthesis and the organic-inorganic interface. *Nature* **2005,** *437* (7059), 664-670.

91. Manna, L.; Scher, E. C.; Alivisatos, A. P., Synthesis of soluble and processable rod-, arrow-, teardrop-, and tetrapod-shaped CdSe nanocrystals. *J. Am. Chem. Soc.* **2000,** *122* (51), 12700-12706.

92. Tang, Z.; Kotov, N. A.; Giersig, M., Spontaneous organization of single CdTe nanoparticles into luminescent nanowires. *Science* **2002,** *297* (5579), 237-240.

93. Wang, F. D.; Dong, A. G.; Sun, J. W.; Tang, R.; Yu, H.; Buhro, W. E., Solution-liquid-solid growth of semiconductor nanowires. *Inorg. Chem.* **2006,** *45* (19), 7511-7521.

94. Phok, S.; Rajaputra, S.; Singh, V., Fabrication of copper indium diselenide nanowires. *Mater. Res. Soc. Symp. Proc.* **2008,** *1031E* (Nanostructured Solar Cells), 1031-H13-28.

95. Liusman, C.; Li, S.; Chen, X.; Wei, W.; Zhang, H.; Schatz, G. C.; Boey, F.; Mirkin, C. A., Free-standing bimetallic nanorings and nanoring arrays made by on-wire lithography. *ACS Nano 4* (12), 7676-7682.

96. Dresselhaus, M.; Lin, Y.-M.; Rabin, O.; Black, M.; Kong, J.; Dresselhaus, G., Nanowires. In *Springer Handbook of Nanotechnology, 2nd ed.*, Bhushan, B., Ed. Springer Berlin Heidelberg: 2007; pp 113-160.

97. Fan, H. J.; Werner, P.; Zacharias, M., Semiconductor nanowires: From self-organization to patterned growth. *Small* **2006,** *2* (6), 700-717.

98. Kuno, M., An overview of solution-based semiconductor nanowires: Synthesis and optical studies. *Phys. Chem. Chem. Phys.* **2008,** *10* (5), 620-639.

99. Sapra, S.; Poppe, J.; Eychmuller, A., CdSe nanorod synthesis: A new approach. *Small* **2007,** *3* (11), 1886-1888.

100. Wooten, A. J.; Werder, D. J.; Williams, D. J.; Casson, J. L.; Hollingsworth, J. A., Solution-liquid-solid growth of ternary Cu-In-Se semiconductor nanowires from multiple- and single-source precursors. *J. Am. Chem. Soc.* **2009,** *131* (44), 16177-16188.

101. Jiang, Y.; Wu, Y.; Mo, X.; Yu, W.; Xie, Y.; Qian, Y., Elemental solvothermal reaction to produce ternary semiconductor $CuInE_2$ (E = S, Se) nanorods. *Inorg. Chem.* **2000,** *39* (14), 2964-2965.

102. Wu, C. C.; Shiau, C. Y.; Ayele, D. W.; Su, W. N.; Cheng, M. Y.; Chiu, C. Y.; Hwang, B. J., Rapid microwave-enhanced solvothermal process for synthesis of $CuInSe_2$ particles and its morphologic manipulation. *Chem. Mater.* **2010,** *22* (14), 4185-4190.

103. Schoen, D. T.; Peng, H. L.; Cui, Y., Anisotropy of chemical transformation from In_2Se_3 to $CuInSe_2$ nanowires through solid state reaction. *J. Am. Chem. Soc.* **2009,** *131* (23), 7973-7975.

104. Tang, J.; Hinds, S.; Kelley, S. O.; Sargent, E. H., Synthesis of colloidal $CuGaSe_2$, $CuInSe_2$, and $Cu(InGa)Se_2$ nanoparticles. *Chem. Mater.* **2008,** *20* (22), 6906-6910.

105. Luo, Y., Synthesis of $CuInSe_2$ and $CuGaSe_2$ hexagonal microplates in oleic acid and oleylamine mixture. *Colloid J.* **2009,** *71* (3), 375-379.

106. Li, B.; Xie, Y.; Huang, J. X.; Qian, Y. T., Synthesis by a solvothermal route and characterization of $CuInSe_2$ nanowhiskers and nanoparticles. *Adv. Mater.* **1999,** *11* (17), 1456-1459.

107. Yang, Y. H.; Chen, Y. T., Solvothermal preparation and spectroscopic characterization of copper indium diselenide nanorods. *J. Phys. Chem. B* **2006,** *110* (35), 17370-17374.

108. Wark, S. E.; Hsia, C. H.; Luo, Z.; Son, D. H., Surfactant effect on the formation of $CuInSe_2$ nanowires in solution phase synthesis. *J. Mater. Chem.* (DOI:10.1039/C1JM10401B).

109. Hochbaum, A. I.; Chen, R.; Delgado, R. D.; Liang, W.; Garnett, E. C.; Najarian, M.; Majumdar, A.; Yang, P., Enhanced thermoelectric performance of rough silicon nanowires. *Nature* **2008,** *451* (7175), 163-167.

110. Martin, P.; Aksamija, Z.; Pop, E.; Ravaioli, U., Impact of phonon-surface roughness scattering on thermal conductivity of thin Si nanowires. *Phys. Rev. Lett.* **2009,** *102* (12), 125503/1-125503/4.

111. Martin, P. N.; Aksamija, Z.; Pop, E.; Ravaioli, U., Prediction of reduced thermal conductivity in nano-engineered rough semiconductor nanowires. *J. Phys. Conf. Ser.* **2009,** *193*.

112. Moore, A. L.; Saha, S. K.; Prasher, R. S.; Shi, L., Phonon backscattering and thermal conductivity suppression in sawtooth nanowires. *Appl. Phys. Lett.* **2008,** *93* (8), 083112/1-083112/3.

113. Wang, F.; Tang, R.; Kao, J. L. F.; Dingman, S. D.; Buhro, W. E., Spectroscopic identification of tri-n-octylphosphine oxide (TOPO) impurities and elucidation of their roles in cadmium selenide quantum-wire growth. *J. Am. Chem. Soc.* **2009,** *131* (13), 4983-4994.

114. Kan, S.; Mokari, T.; Rothenberg, E.; Banin, U., Synthesis and size-dependent properties of zinc-blende semiconductor quantum rods. *Nat. Mater.* **2003,** *2* (3), 155-158.

115. Parkes, J.; Tomlinson, R. D.; Hampshire, M. J., Crystal data for copper indium diselenide. *J. Appl. Crystallogr.* **1973,** *6* (5), 414-416.

116. Boehnke, U. C.; Kuehn, G., Phase relations in the ternary system copper-indium-selenium. *J. Mater. Sci.* **1987,** *22* (5), 1635-1641.

117. Fearheiley, M. L., The phase relations in the copper, indium, selenium system and the growth of $CuInSe_2$ single crystals. *Sol. Cells* **1986,** *16* (1-4), 91-100.

118. Shen, J.; Kim, W. K.; Shang, S.; Chu, M.; Cao, S.; Anderson, T. J., Thermodynamic description of the ternary compounds in the Cu-In-Se system. *Rare Met.* **2006,** *25* (5), 481-487.

119. Lou, W. J.; Wang, X. B.; Chen, M.; Liu, W. M.; Hao, J. C., A simple route to synthesize size-controlled Ag_2S core-shell nanocrystals, and their self-assembly. *Nanotechnology* **2008,** *19* (22), 225607/1-225607/8.

120. Lu, X. M.; Tnan, H. Y.; Korgel, B. A.; Xia, Y. N., Facile synthesis of gold nanoparticles with narrow size distribution by using AuCl or AuBr as the precursor. *Chem. Eur. J.* **2008,** *14* (5), 1584-1591.

121. Shukla, N.; Liu, C.; Jones, P. M.; Weller, D., FTIR study of surfactant bonding to FePt nanoparticles. *J. Magn. Magn. Mater.* **2003,** *266* (1-2), 178-184.

122. Cotton, F. A.; Barnes, R. D.; Bannister, E., Effect of complex formation by phosphine oxides on their P-O stretching frequencies. *J. Chem. Soc.* **1960**, 2199-2203.

123. Katari, J. E. B.; Colvin, V. L.; Alivisatos, A. P., X-ray photoelectron spectroscopy of CdSe nanocrystals with applications to studies of the nanocrystal surface. *J. Phys. Chem.* **1994,** *98* (15), 4109-4117.

124. Young, A. G.; Al-Salim, N.; Green, D. P.; McQuillan, A. J., Attenuated total reflection infrared studies of oleate and trioctylphosphine oxide ligand adsorption and exchange reactions on CdS quantum dot films. *Langmuir* **2008,** *24* (8), 3841-3849.

125. Manna, L.; Wang, L. W.; Cingolani, R.; Alivisatos, A. P., First-principles modeling of unpassivated and surfactant-passivated bulk facets of wurtzite CdSe: A model system for studying the anisotropic growth of CdSe nanocrystals. *J. Phys. Chem. B* **2005,** *109* (13), 6183-6192.

126. Shukri, Z. A.; Champness, C. H., Cleavage and twinning in $CuInSe_2$ crystals. *Acta Crystallogr., Sect. B: Struct. Sci.* **1997,** *53*, 620-630.

127. Materials Studio, A. S., Inc.

128. Wang, Z. W.; Li, Z. Y., Structures and energetics of indium-catalyzed silicon nanowires. *Nano Lett.* **2009,** *9* (4), 1467-1471.

129. Yu, H.; Buhro, W. E., Solution-liquid-solid growth of soluble GaAs nanowires. *Adv. Mater.* **2003,** *15* (5), 416-419.

130. Trentler, T. J.; Hickman, K. M.; Goel, S. C.; Viano, A. M.; Gibbons, P. C.; Buhro, W. E., Solution-liquid-solid growth of crystalline III-V semiconductors: an analogy to vapor-liquid-solid growth. *Science* **1995,** *270* (5243), 1791-1794.

131. Khanna, P. K.; Jun, K. W.; Hong, K. B.; Baeg, J. O.; Chikate, R. C.; Das, B. K., Colloidal synthesis of indium nanoparticles by sodium reduction method. *Mater. Lett.* **2005,** *59* (8-9), 1032-1036.

132. Liu, G.; Bard, A. J., Rapid preparation and photoelectrochemical screening of $CuInSe_2$ and $CuInMSe_2$ arrays by scanning electrochemical microscopy. *J. Phys. Chem. C* **2010,** *114* (41), 17509-17513.

133. Radue, C.; van Dyk, E. E.; Macabebe, E. Q., Analysis of performance and device parameters of CIGS PV modules deployed outdoors. *Thin Solid Films* **2009,** *517* (7), 2383-2385.

VITA

Name: Stacey Elaine Wark

Address: Department of Chemistry
c/o Dr. Dong Hee Son
Texas A&M University
PO Box 30012
College Station, TX 77843-3012

Email Address: staceywark@hotmail.com

Education: B.S., Chemistry, The University of Dallas, 2005
Ph.D., Chemistry, Texas A&M University, 2011

Publications:

1. Wark, S. E.; Hsia, C. H.; Luo, Z.; Son, D. H., Surfactant effect on the formation of $CuInSe_2$ nanowires in solution phase synthesis. *J. Mater. Chem.* **2011**, DOI:10.1039/C1JM10401B
2. Diaz, A.; David, A.; Perez, R.; Gonzalez, M. L.; Baez, A.; Wark, S. E.; Zhang, P.; Clearfield, A.; Colon, J. L., Nanoencapsulation of Insulin into Zirconium Phosphate for Oral Delivery Applications. *Biomacromolecules* **2010,** *11* (9), 2465-2470.
3. Chan, Y. H.; Chen, J. X.; Liu, Q. S.; Wark, S. E.; Son, D. H.; Batteas, J. D., Ultrasensitive Copper(II) Detection Using Plasmon-Enhanced and Photo-Brightened Luminescence of CdSe Quantum Dots. *Anal Chem* **2010,** *82* (9), 3671-3678.
4. Chen, J. X.; Chan, Y. H.; Yang, T. L.; Wark, S. E.; Son, D. H.; Batteas, J. D., Spatially Selective Optical Tuning of Quantum Dot Thin Film Luminescence. *J Am Chem Soc* **2009,** *131* (51), 18204-+.
5. Chan, Y. H.; Chen, J. X.; Wark, S. E.; Skiles, S. L.; Son, D. H.; Batteas, J. D., Using Patterned Arrays of Metal Nanoparticles to Probe Plasmon Enhanced Luminescence of CdSe Quantum Dots. *Acs Nano* **2009,** *3* (7), 1735-1744.
6. Chen, J. X.; Liao, W. S.; Chen, X.; Yang, T. L.; Wark, S. E.; Son, D. H.; Batteas, J. D.; Cremer, P. S., Evaporation-Induced Assembly of Quantum Dots into Nanorings. *Acs Nano* **2009,** *3* (1), 173-180.
7. Wark, S. E.; Hsia, C. H.; Son, D. H., Effects of ion solvation and volume change of reaction on the equilibrium and morphology in cation-exchange reaction of nanocrystals. *J Am Chem Soc* **2008,** *130* (29), 9550-9555.